Published in final edited form as:

FASEB J. 2020 May ; 34(5): 6166–6184. doi:10.1096/fj.201901920R.

Flow-Regulated Endothelial Glycocalyx Determines Metastatic Cancer Cell Activity

Solomon A. Mensah[1,6], **Alina A. Nersesyan**[1,6], **Ian C. Harding**[1], **Claire I. Lee**[1], **Xuefei Tan**[2], **Selina Banerjee**[3], **Mark Niedre**[1,2], **Vladimir P. Torchilin**[4], **Eno E. Ebong**[1,3,5,‡]

[1]Department of Bioengineering, Northeastern University, Boston, MA

[2]Department of Electrical and Computer Engineering, Northeastern University, Boston, MA

[3]Department of Chemical Engineering, Northeastern University, Boston, MA

[4]Department of Pharmaceutical Science, Northeastern University, Boston, MA

[5]Neuroscience Dept., Albert Einstein College of Medicine, New York, NY

[6]These authors made equal contributions to this work.

Abstract

Cancer metastasis and secondary tumor initiation largely depend on circulating tumor cell (CTC) and vascular endothelial cell (EC) interactions by incompletely understood mechanisms. Endothelial glycocalyx (GCX) dysfunction may play a significant role in this process. GCX structure depends on vascular flow patterns, which are irregular in tumor environments. This work presents evidence that disturbed flow (DF) induces GCX degradation, leading to CTC homing to the endothelium, a first step in secondary tumor formation. A 2-fold greater attachment of CTCs to human ECs was found to occur in DF conditions, compared to uniform flow (UF) conditions. These results corresponded to an approximately 50% decrease in wheat germ agglutinin (WGA) labeled components of the GCX in DF conditions, versus UF conditions, with undifferentiated levels of CTC-recruiting E-selectin in DF versus UF conditions. Confirming the role of the GCX, neuraminidase induced degradation of WGA-labeled GCX in UF cell culture conditions or in Balb/C mice led to an over 2-fold increase in CTC attachment to ECs or to Balb/C mouse lungs, respectively, compared to untreated conditions. These experiments confirm that flow-induced GCX degradation can enable metastatic CTC arrest. This work, therefore, provides new insight into pathways of secondary tumor formation.

Keywords

Endothelial Cells; Metastatic Cancer Cells; Disturbed Flow; Glycocalyx; Intercellular Interactions

‡**Correspondence:** Eno. E. Ebong, PhD., Department of Chemical Engineering, Northeastern University, 360 Huntington Avenue, 313 Snell Engineering Building, Boston, MA 02115, Phone: 617-373-8744, Fax: 617-373-2209, e.ebong@northeastern.edu.

Author Contributions

S.A.M. and E.E.E. designed the experiments. S.A.M., A.A.N., I.C.H., C.I.L., X.T., and S.B. performed the experiments and analyzed the data. S.A.M., A.A.N., I.C.H., V.P.T., M.N., and E.E.E. interpreted the results of the experiments. S.A.M., A.A.N., S.B., and E.E.E drafted the figures and manuscript. S.A.M., A.A.N., I.C.H., and E.E.E. edited, revised, and approved the final manuscript. V.P.T., M.N., and E.E.E. supervised the project.

Conflicts of Interest: The authors declare no conflict of interest.

1. INTRODUCTION

The metastatic spread of cancer is the leading cause of cancer related deaths globally [1, 2]. A common therapeutic approach to addressing this problem has involved targeting the leaky blood vessel network of primary tumors to prevent tumor cells from escaping into the blood stream [3, 4]. New therapies to treat cancer metastasis and invasiveness will need to mitigate secondary tumor formation once tumor cells have already entered the blood stream. However, the mechanisms leading to the initiation of secondary tumors by metastatic and invasive cancer remain elusive.

In late stage cancer, circulating tumor cells (CTCs), having escaped from primary tumors (Fig. 1A), can be detected in peripheral blood flow of human patients [5, 6]. This indicates that CTCs are able to survive in the bulk blood flow environment and maneuver their way through complex geometries within the vasculature of human hosts [7]. Eventual metastasis is site specific and known to preferentially occur at areas where there is increased chemokine activity. Vessel geometry is also an important factor, and attention has been focused on small diameter capillary vessels in which CTCs transition from rolling in their motion to bullet type motion, leading to their reduced velocity and firm adherence to the capillary wall even in the presence of weak adhesion forces [8]. Abrupt changes in vessel geometry have also been implicated in the progression of disease and metastatic specificity [9], although understudied. These geometric irregularities or non-uniformities affect blood flow patterns and result in the formation of disturbed flow (DF) regions (Fig. 1C and 1E) within blood vessels. DF regions are prevalent in distant organs where metastasis is more likely to occur, due to the high frequency of branched or curved blood vessel in these organs [10, 11], which includes the lungs, the liver, and several other organs [12]. The branches and curves, as suggested by Guo et al., exhibit localized vorticity and shear rate which are different from straight sections of the vessel [13]. This suggests that the hemodynamic factors in branched or curved areas are relevant to the spread of cancer. DF erodes the blood vessel by activating molecular signaling that causes inflammation and damage to the endothelial cells (ECs) that line the blood vessel wall, leading to pathogenic conditions [14–17]. The presence of DF also affects vascular permeability and recruitment of cells from the blood compartment to the endothelium [15]. Therefore, DF could be very relevant in the formation of secondary tumors.

We, therefore, hypothesize that DF conditions can promote CTC attachment to EC-covered blood vessel walls, followed by migration into surrounding tissue and leading to secondary tumor formation (Fig. 1B) [7]. We also hypothesize that CTC clustering can be enhanced by DF conditions, as CTC clustering is a very important phenomenon that enhances their survival in the blood stream. In addition, as shown by human pathology studies, CTCs invade host tissues as strands, cords and clusters [18], which ensures proliferation into secondary tumors. DF-induced CTC clustering and subsequent migration through the endothelium could be a possible pathway leading to cancer progression [19, 20].

ECs are covered by glycocalyx (GCX), which is a complex sugar coat. Due to its unique position, the GCX lines the luminal side of blood vessels and plays an essential role as a

vasculoprotective barrier [21–23]. While there have been numerous studies focusing on DF-induced endothelial dysfunction, only a few studies have paid attention to DF regulation of the GCX structure and function [24–27] despite its importance in vascular homeostasis. Recently, Harding *et al* labeled heparan sulfate, a major component of GCX, to determine the effects of DF on GCX structure and function compared to the effects of uniform flow (UF) conditions [24]. It was found that DF destabilizes the GCX and consequently disrupts the expression and localization of caveolin-1, potentially leading to blockage of endothelial nitric oxide synthase (eNOS) activation [24].

Relevant to CTC attachment to EC-covered blood vessel walls, other major GCX components like sialic acid (SA) are of great importance because of their role in cell and molecular recognition [28]. To our knowledge, studies investigating the activities of CTCs in relation to degradation of the GCX as a whole, or in relation to degradation of its SA sub-component, are limited. Recently, we performed a study in which ECs were treated with GCX degradative enzyme, neuraminidase (Neur), to cleave various SA residues of the GCX and to determine their correlation to enhanced cancer attachment to the endothelium [29]. We concluded that the ∝−2,6-linked residue of SA is the first to be degraded in the presence of Neur, resulting in vulnerability of the GCX layer, which is sufficient to initiate CTC attachment to the endothelium [29]. Whether DF will have the same effects as Neur, by degrading SA and leading to enhanced attachment of CTCs to the endothelium, is unknown. Answering this question will be of great clinical importance.

Adhesion molecules on the endothelium play a significant role in CTC migration across the endothelium [30, 31]. They enhance CTC binding during attachment, consistent with how leukocytes attach to the endothelium [32]. GCX and these adhesion molecules, especially E-selectin, are similarly positioned as transmembrane glycoproteins within the endothelium [1]. EC GCX thickness ranges from 0.02 to 10 μm depending on species size, vascular bed, the microenvironment niche, *in vivo* versus *in vitro* conditions, and the GCX preservation and visualization approach used [33]. The E-selectin adhesion molecule extends to 0.03 to 0.07 μm on cell surfaces [34]. The height differences between healthy GCX and E-selectin suggest that CTC ligands will find it difficult to access E-selectin adhesion receptors on the endothelium (Fig. 1D and 1E) [35]. By regulating the expression of GCX through DF or enzyme activity, we hope to learn more about the mechanism of interaction between ECs and CTCs.

Here we report for the first time the effects of DF-induced endothelial GCX degradation, versus E-selectin coverage, on the attachment of cancerous cells to the endothelium. Our results bring to light a GCX-mediated pathway to secondary tumor formation. Furthermore, this work suggests that the creation of endothelial GCX reinforcing drugs, specifically targeted to the DF areas of the vasculature, may reduce the metastatic potential of CTCs.

2. MATERIALS AND METHODS

2.1 Cell Culture

Human umbilical vein ECs (HUVEC; Fig. S1), purchased from ATCC (Manassas, VA), were used at passages 2 to 8. HUVEC were seeded at a density of 15,000 – 20,000 cells/cm^2

on 0.17 mm-thick 22 mm x 40 mm rectangular coverslips coated with 60 μg/ml of fibronectin. HUVEC were cultured with Vascular Cell Basal Medium. The medium was supplemented with recombinant human vascular endothelial growth factor (rh VEGF: 5 ng/mL), epidermal growth factor (rh EGF: 5 ng/mL), basic fibroblast growth factor (rh FGF basic: 5 ng/mL), and insulin-like growth factor-1 (rh IGF-1: 15 ng/mL). Additional supplements included L-glutamine (10 mM), heparin sulfate (0.75 Units/mL), hydrocortisone (1 μg/mL), ascorbic acid (50 μg/mL), and fetal bovine serum (FBS: 2%). The medium and supplements were all purchased from ATCC. HUVEC reached 100% confluency at 3 to 4 days after seeding.

Two different types of CTCs were used. 4T1 mouse metastatic breast cancer cells (ATCC) were cultured in Dulbecco's Modified Eagle Medium (purchased from Invitrogen) with 1% penicillin-streptomycin and 10% FBS (Gibco Life Technologies). MCF-7 human metastatic breast cancer cells (ATCC) were cultured in Eagle's Minimum Essential Medium (purchased from ATCC) with 0.01 mg/ml of human recombinant insulin (Gibco) and 10% FBS.

All cultured ECs and CTCs were maintained in a humidity-controlled environment at 37°C with 5% CO_2.

2.2 Application of Flow Conditions in Cell Culture Studies

To introduce DF and UF to HUVEC, a vertical step flow chamber, designed and manufactured in our lab, was used (Fig. 2A and Fig. S1) [24]. HUVEC monolayers cultured on glass slides as described above were inserted into a recess in the bottom chamber downstream from the step (Fig. 2A). The DF flow region, through SolidWorks simulations, was previously confirmed to consist of a reversal in flow direction, a high shear stress gradient, and shear stress ranging from −8 dynes/cm^2 to 12 dynes/cm^2 [24]. UF flow conditions consists of a shear stress of 12 dynes/cm^2. Computer simulations (Fig. S2A) also revealed a transition region from DF to UF. In this transition region flow streamlines appear via the naked eye to be UF, while the flow parameters are not yet uniform and are gradually approaching uniformity (Fig. S2A).

The flow setup was placed in a humidity-controlled environment at 37°C and 5% CO2. HUVEC monolayers were exposed to flow for 4 hours using the supplemented Vascular Cell Basal Medium, with the addition of 0.5% of bovine serum albumin (BSA), to stabilize the GCX. For assessment of E-selectin expression, 0.4 ng/ml of tumor necrosis factor-α (TNF-α) was also incorporated (Fig. S1) into the 4-hour flow experiment to make E-selectin immune-detectable (Fig. S3A and S3B) without affecting the health and integrity of the endothelial cells and the glycocalyx (Fig. S3C and S3D). A negative control without TNF-α was also done to confirm the need for TNF-α-mediated detection of E-selectin and to confirm that the low level of TNF-α minimally affects the GCX as compared to higher levels of TNF-α used in prior published studies (Fig. S3A–S3D) [1, 36]. When CTCs were added to the flow stream, for the purposes of enabling CTC attachment to ECs, shear stress was reduced to 1 dyne/cm^2 for 1 hour after the 4-hour UF and DF pre-conditioning period was completed (Fig. S1). This reduced flow condition best mimics flow conditions that are relevant where CTCs approach the vessel wall *in vivo*, as previously reported [1, 37–39]. Moreover, it minimizes the eddy current region so that CTC residence time over DF-

conditioned ECs more closely matches CTC residence time over UF-conditioned ECs (Fig. S2B), as the effect of eddy current on CTCs was outside of the scope of our study. Furthermore, this reduced flow removed direct impact of flow on regulation of CTC attachment (Fig. S2C), as we were only interested in studying the impact of the flow-regulated GCX.

2.3 Neuraminidase Enzyme Treatment in Cell Culture Studies

Neuraminidase (Neur) enzyme from *clostridium perfringens* was used to target the N-acetyl-neuraminic components of GCX in order to degrade all the forms of SA present in GCX. To achieve this, regular growth media from cultured HUVEC was replaced with media containing Neur enzyme at a concentration of 0 mU/ml (for control UF/untreated conditions) or 15 mU/ml (Fig. S1). The two concentrations of Neur, were selected after a careful pilot study of the effects of 0 mU/ml, 15 mU/ml, 135 mU/ml, 1215 mU/ml and 3645 mU/ml of Neur, to determine the appropriate enzyme concentration (Fig. S4). 15mU/ml of Neur was chosen because it was found to best maintain cell viability during flow experiments while significantly degrading SA. 0 mU/ml will not degrade SA. The Neur-modified culture media was used during UF experiments only (Fig. S1).

2.4 In Vitro Cancer Cell Labeling, Attachment Assay, Imaging, and Quantification

CTCs (4T1 or MCF7) were cultured as described above. Prior to the performance of attachment assays, 10^3/ml of suspended CTCs were labeled with 15μM CellTracker Red CMTPX Dye (Thermo Fisher Scientific) for easy identification during co-culture experiments. The CellTracker-labeled CTCs were then injected into the parallel plate flow stream for co-incubation with HUVEC, as mentioned above (Fig. S1). For the set of experiments related to Neur studies, effort was made to ensure that Neur impacted only ECs and not CTCs. To achieve this, HUVEC were removed from the UF/untreated or UF/Neur environment and the CellTracker-labeled CTCs were co-incubated with UF/untreated- and UF/Neur-conditioned HUVEC under static conditions for 1 hour in Neur-free media (Fig. S1). After HUVEC and CTC co-incubation, whether under flow or static conditions, non-attached cells were removed by washing with growth media.

A Zeiss Z1 Axio Observer fluorescence microscope with a 10x magnification objective was used to capture CTC and EC interactions. For each attachment experiment, 6 different fields of view were captured with an excitation wavelength of 558 nm to locate red CellTracker-labeled CTCs. Brightfield images were also captured to determine the health of HUVEC. NIH Image J and a cell counter plug-in was used to count the number of attached CTCs. In addition, CTC clusters were quantified, by counting the number of groups of two or more cells together. Lastly, the total number of CTCs that initiated migration through the endothelium were considered as cells that appeared to be in the same or similar focal plane as the HUVEC, because, due to the presence of the glass slide, CTCs were not able to completely cross and migrate away from the endothelial layer. The total number of CTCs that initiated migration through the endothelium was determined by using the working distance of the microscope, marking the HUVEC level as the baseline and considering only 4T1 or MCF7 cells that were near baseline as cells initiating migration (Fig. S5A). We confirmed EC-CTC interactions using orthogonal views from confocal images. Fig. S5B

shows clustered CTC cells attached to the surface of ECs. Movement of CTCs through HUVEC was also observed from orthogonal views (Fig. S5C). We also used the Z-stack function on the confocal, and orthogonal views, to confirm that cancer cells were stationed near but beneath the endothelial layer (Fig. S5D, S5E). CTC attachment, clustering, and migration results were all normalized with data obtained from conditions of UF in the absence of Neur.

2.5 GCX, E-selectin, and VE-cadherin Labeling, Imaging, and Quantification for Cell Culture Studies

After various treatment conditions, we assessed structural changes in GCX caused by conditions of UF, DF, or UF with Neur (Fig. S1). First, HUVEC monolayers were fixed with 2% paraformaldehyde (PFA) combined with 0.1% glutaraldehyde in phosphate buffered saline (PBS), for 30 minutes at room temperature (RT). To label the GCX, HUVEC were incubated for an hour at 4^{o}C with 5–20 μg/ml biotinylated wheat germ agglutinin (WGA; Vector Labs) lectin in PBS with 3% BSA to block nonspecific binding. WGA largely tags the SA component of the GCX, although it has affinity for other components [40–43]. A concentration of 1:1000 of Alexa flour 488-conjugated anti-biotin was used for secondary detection.

For E-selectin staining (Fig. S1), HUVEC monolayers were fixed with 4% paraformaldehyde in PBS, for 20 minutes at RT. Fixed cells were incubated overnight at 4°C with human E-selectin antibody (R&D Systems) at a concentration of 10 μg/ml in a solution of 10% goat serum in PBS to block non-specific staining. Secondary labeling was performed by incubation with 1:1000 concentrated biotinylated goat anti mouse IgG (H+L) highly cross adsorbed secondary antibody, for 1 hour at RT. E-selectin, which is 0.03 to 0.07 μm tall [34], cannot easily be visualized via confocal microscopy because the confocal microscope is able to resolve objects at approximately 0.20 μm in size and larger. To overcome this limitation and image E-selectin using confocal microscopy, our prior application of TNF-α was not sufficient and one more step was needed, which involved immunocytochemical signal amplification. Signal amplification was performed via tertiary labeling with 1:1000 concentrated Alexa Flour 488-conjugated anti-biotin, for 1 hour at RT.

For VE-cadherin staining, HUVC were fixed with 4% paraformaldehyde and incubated with Alexa Flour 647-conjugated anti-human VE-cadherin (CD144) antibody (obtained from Biolegend) at a concentration of 5 μg/ml in 2% BSA blocking solution.

GCX, E-selectin, and VE-cadherin labeled samples were covered with Vectashield anti-fade mounting medium (Vector Labs), containing 4’,6-diamidino-2-phenylindole (DAPI) to label cell nuclei. Samples were then sealed in preparation for imaging and quantification.

Confocal microscopy (Fig. S1) provided enhanced resolution and allowed for the capturing of different planes within our cell monolayers, which were later reconstructed into a three-dimensional (3D) image. For this process a Zeiss LSM 700 confocal microscope with a 63x oil objective with excitation wavelengths of 490 nm (for WGA or E-selectin), 650 nm (for VE-cadherin), and 350 nm (for DAPI) was utilized to obtain XY-plane slices. Intervals for slices were 0.2 μm. Using NIH Image J software, these slices were reconstructed into

complete 3D images. WGA or E-selectin coverage of the surface of endothelial monolayers was quantified from the z-projected *en face* view of the 3D image. The total area of WGA or E-selectin fluorescence was measured, and this measurement was divided by the total area of the field of view. WGA thickness was also quantified. In cross-sectional views derived from the 3D images, lines were drawn perpendicular to the cell surface, from the top of the WGA fluorescence to its base. The length of the lines was measured to represent the thickness of WGA on the surface of HUVEC monolayers. For E-selectin, on the other hand, thickness was not quantified. Since E-selectin signal was amplified for visualization, unlike WGA signal that was not amplified for visualization, E-selectin thickness measurements were not an appropriate analysis method to implement here. VE-cadherin was qualitatively assessed to confirm EC-to-EC contact, which is indicative of EC layer integrity.

2.6 Overview of Animal Studies

All animal studies were done in accordance with the regulations of the Institutional Animal Care and Use Committee (IACUC) at Northeastern University, under protocol number 18–0725R. Eight male 6–8-week-old BALB/C mice were obtained from Jackson Laboratories. The animals were fed a regular chow diet for 1 week before commencing the experiments. Four mice were studied for control experiments and four mice were studied for Neur treatment experiments, to determine the *in vivo* effect of enzyme treatment on GCX and CTC attachment at locations prone to secondary tumor formation.

2.7 Neuraminidase Enzyme Treatment in Animals

Animals were weighed to calculate the volume of blood. The volume of blood informed the volume of enzyme to inject in order to achieve the desired concentration. Control animals were intravenously injected with saline. Neur-treated mice were intravenously injected with 5U/mL of Neur. Animals were allowed 14 hours to recover before further experimentation.

2.8 Cancer Cell Injection and Enumeration in Animals

After 14 hours, both control and Neur-treated mice were intravenously injected with 10^6 CTCs in 200μL of phenol free media via the tail vein. 4T1 CTCs were chosen to match the species of the animal. These cells were labeled with far-red CellTrace (Thermo Fisher Scientific), which is similar to the red CellTracker that was used for the cell culture studies but easier to measure *in vivo* using the diffuse *in vivo* flow cytometery (DiFC) [44–47] technique.

We performed DiFC (Fig. S6A), which is a new technique to detect rare fluorescently labeled cells moving in the blood stream in highly scattering biological tissue, to investigate the *in vivo* clearance kinetic of the CellTrace labeled 4T1 CTCs. After the mice were injected with the cells they were scanned by DiFC for 15 minutes at multiple time points (10, 30 and 60 minutes) after the injection. During each scan, the injected mouse was kept anesthetized under isoflurane and the tail was secured with a custom-made holder (Fig. S6C). We placed the DiFC probe on the ventral surface of the tail about 3 cm from the mouse body, approximately above the ventral caudal vascular bundle (Fig. S6C). DiFC uses two custom designed groupings of optical fibers consisting of a central ‘source’ fiber and eight fluorescence collection fibers, as well as integrated optical filters and collection lens

[46] (Fig. S6A). The DiFC probe was placed in firm contact with the skin, to prevent motion artifacts during scanning (Fig. S6). A heating pad was also placed over the exposed area of the mouse tail during the scanning to maintain blood flow. As each fluorescently labeled CTC passed through the field of view of the probe, a transient fluorescence pulses were detected as in our previous work (Fig. S6B). Using a custom-developed signal-processing algorithm [45], we analyzed the DiFC data to determine the rate of CTCs in the blood stream (counts per minute) and the average peak amplitude (linearly related to the brightness of individual cells) during scanning. DiFC distinguishes cells moving in arterial venous directions (forward and reverse) which mitigates double counting of CTCs (Fig. S6). A noticeable decrease in CTCs in the blood stream was taken to indicate CTC clearance from the blood. After 60 minutes, the mice were euthanized.

2.9 Animal Euthanization, Tissue Dissection, and Fluorescent Staining

Each mouse was injected with ketamine and xylazine anesthetics based on their weight. The hind limbs were pinched to ensure that each mouse was completely under anesthesia. A surgical incision was made from the abdominal wall to the thoracic wall of the mouse to expose the heart. Using a small needle inserted into the heart, the vessels of each mouse were pressure perfused with 2% BSA in PBS to euthanize by exsanguination while preventing the GCX from collapsing. Once exsanguination was complete, 4% PFA in PBS was pressure perfused to fix the vessels. The lungs and abdominal aorta were excised.

The lungs, a well-established site of secondary tumor formation, were refrigerated in PBS. Thanks to the auto fluorescence of the lung tissue and prior fluorescent labeling of the CTCs, no further staining was required. The lungs could be immediately imaged to count the number of attached fluorescent CTCs in the absence and presence of Neur.

Some segments of excised abdominal aortas were refrigerated in PBS. Later, the aortas were longitudinally cut to expose the luminal vessel wall *en face* and to verify the integrity of the endothelium in the absence and presence of Neur. On the luminal vessel wall, endothelium markers were immunolabeled using antibodies against zonula occludens-1 (ZO-1; Fisher), eNOS (Fisher), platelet endothelial cell adhesion molecule-1 (PECAM-1; Novus Biologicals), and E-selectin (Fisher). Immunostaining was done as previously described [24]. Secondary detection was achieved by incubating samples in Alexa Flour 488-conjugated goat anti-rabbit secondary antibody. The stained *en face* tissue was covered with Vectashield anti-fade medium containing DAPI and sealed before imaging.

Remaining excised abdominal aortas were frozen in optimum cutting temperature media (OCT) and stored at −80ºC. A Leica cryostat was used to create 6-μm thin axial sections of the frozen aortas. The thin sections were mounted and allowed to dry out on positively charged glass slides (Fisher Scientific). The aorta sections were later stained and imaged to quantify GCX expression in the presence and absence of Neur. As before, WGA was used as a marker of GCX. Sections were then incubated in 1:100 biotinylated WGA in 5% BSA for 2 nights. Secondary detection of WGA-labeled GCX was achieved by incubating sections in 1:500 HRP-conjugated streptavidin (Thermo Scientific) for 1 hour, which was amplified using 1:100 of TSA Plus Cyanin 3 (Perkin Elmer) for 7 minutes. DAPI and Vectashield anti-fade mounting medium were applied before imaging.

2.10 Imaging and Analysis in Animal Studies

WGA-labeled GCX in aorta sections were visualized using a Zeiss LSM 710 Confocal Laser Scanning microscope at 63X/oil magnification. GCX coverage and thickness were quantified as previously described [17]. ZO-1, PECAM-1, E-selection, and eNOS labeled *en face* aorta tissue samples were also visualized by confocal microscopy, using a 40x/water objective and a 490 nm excitation filter for green signal [24]. Whole excised lungs after experimentation were mounted on glass sides without mounting media and imaged using a Zeiss LSM 710 Confocal Laser Scanning microscope at 40X/water objective. A red filter of excitation of 558 nm was used to identify Cell Trace labeled 4T1 cells attached to the lungs.

2.11 Statistics

Data is expressed as means ± SEM. Graph Pad Prism was used for all statistical analysis and determination of statistical significance of differences between means. Additional details of the statistical tests are described in figure captions.

3. RESULTS

3.1 Interactions between CTCs and the endothelium are increased in DF conditions

HUVEC exposed to both UF and DF patterns (Fig. 2A) did not show any morphological changes after 4 hours of conditioning with flow (Fig. 2B and 2C) when compared to HUVEC in static conditions (Fig. S3E). We also confirmed endothelium integrity by immunostaining for VE-cadherin junctional protein. This qualitative immunocytochemical evaluation of VE-cadherin (Figs. 2B and 2C, and Fig. S3E) confirmed that the endothelium was intact after HUVEC were exposed to DF, UF, and static conditions. In static conditions, when CellTracker-labeled 4T1 cells were co-incubated with HUVEC, approximately 11 4T1 CTCs were attached per every thousand ECs (Fig. S2C). CellTracker-labeled 4T1 CTCs were also co-incubated with 4-hour 12 dynes/cm^2 flow-conditioned HUVEC monolayers, for 1 hour at a reduced flow rate of 1 dyne/cm^2. Under UF conditions we observed an attachment of approximately 6 4T1 cells for every thousand ECs. Normalized, 4T1 CTC attachment to the endothelium was at a level of 1.00 ± 0.06 (Fig. 2D and 2F). In the DF region of the flow chamber, a normalized number of 2.35±0.29 cells were attached per field of view (Fig. 2D and 2F). This represents a statistically significant 2-fold increase in the attachment of 4T1 CTCs to HUVEC in DF conditions compared to UF conditions. We investigated the rate of clustering of 4T1 CTCs after co-incubation with HUVEC monolayers under flow conditions. The normalized data, under UF conditions, was 1.00 ± 0.09 clusters of 4T1 CTCs on HUVEC (Fig. 2D and 2G). With introduction of HUVEC to DF conditions, the clustering of 4T1 CTCs was at 3.19 ± 0.63 (Fig. 2D and 2G), representing a significant 3-fold increase with DF compared to UF conditions. Migration of cancer cells through the endothelium is important for secondary tumor formation. We therefore quantified the extent of initiated migration of 4T1 breast cancer cells through the endothelium. In UF conditions the extent of initiated migration was normalized to 1.00±0.09 (Fig. 2D and 2H). The presence of DF on HUVEC monolayers resulted in a significant increase in the initiated migration of 4T1 breast cancer cells through the endothelium, with the normalized value of initiated migration reaching 3.66 ± 1.22 (Fig. 2D and 2H).

Similar results were observed when we matched the endothelium species with the CTC species, by utilizing MCF7 CTCs in place of 4T1 CTCs. In static conditions, when CellTracker-labeled MCF7 cells were co-incubated with HUVEC, approximately 20 MCF7 CTCs were attached per every thousand ECs. Under UF conditions we observed an attachment of approximately 11 MCF7 cells for every thousand ECs. The normalized data for MCF7 CTC attachment to the endothelium under UF conditions was 1.00 ± 0.24 (Fig. 2E and 2F). Exposure to DF resulted in a significant 2.3-fold increase in the attachment of MCF7 cells to HUVEC, with the normalized value of attachment increasing to 2.34 ± 0.42 (Fig. 2E and 2F). The level of clustering of MCF7 CTCs on HUVEC was at 1.00 ± 0.41 for UF (Fig. 2E and 2G). After HUVEC exposure to DF, MCF7 CTC clustering significantly increased to a normalized value of 2.49 ± 0.44 (Fig. 2E and 2G). Unlike 4T1 CTCs, when the initiated migration of MCF7 CTCs across the endothelial barrier in UF conditions was compared to DF conditions the difference was statistically insignificant. The normalized level for UF conditions was at 1.00 ± 0.16 (Fig. 2E and 2H) and for DF conditions was at 1.66 ± 0.39 (Fig. 2E and 2H).

For a control experiment, after flow-conditioning ECs we co-incubated them with CTCs under static conditions and not in 1 dyne/cm^2 flow conditions (Fig. S7). This control experiment verified that the CTC-EC co-incubation via 1 dyne/cm^2 did not limit the opportunity for CTC attachment, clustering and migration, which one might expect due to reduced CTC residence time that exists in 1 dyne/cm^2 conditions compared to static conditions.

3.2 The high levels of CTC interactions with DF-condition endothelium coincide with endothelial GCX degradation but no change in E-selectin coverage

To determine whether increased cancer cell attachment to the endothelium could occur as a result of GCX changes, the GCX was visualized by labeling it with fluorescently-tagged WGA, which labels primarily the SA component of the GCX [40, 41]. The GCX was found to be intact on the surface of HUVEC monolayers even in static (no flow) conditions (Fig. S3C and S3D). Under UF conditions, WGA-labeled GCX covered 88.65 ± 4.35% of HUVEC monolayers, represented by a normalized value of 1.00 ± 0.07 (Fig. 3A, 3C, and 3F). The WGA-labeled GCX thickness was 1.57 ± 0.15μm, represented by a normalized value of 1.00 ± 0.14 (Fig. 3A, 3C, and 3G). After introducing HUVEC monolayers to DF patterns, the normalized GCX coverage for the DF area decreased to 0.44 ± 0.01 (Fig. 3A, 3B, and 3F). Normalized thickness at the DF area was also 0.41 ± 0.08 (Fig. 3A, 3B, and 3G). This is a statistically significant difference in GCX coverage and thickness in the DF conditions, compared to the UF condition.

To determine whether cancer cell attachment to the endothelium could be due to increased adhesion receptor expression, we analyzed the coverage of ECs by E-selectin in static, DF and UF conditions using immunostaining. In static conditions, E-selectin was barely expressed (Fig. S3A). The normalized E-selectin coverage in the UF region was 1.00±0.19 (Fig. 3A, 3E, and 3H). After introducing DF to HUVEC monolayers, normalized E-selectin coverage was 1.29±0.29 (Fig. 3A, 3D, and 3H). representing a nonsignificant change in expression of E-selectin adhesion molecules between DF and UF regions. Although western

blots would have been useful in this case to better quantify E-selectin, it was out of the scope of this study due to the complexity of the flow and animal experiments.

3.3 Introducing GCX-degrading Neur into the UF environment results in an increase in CTC interactions with the endothelium; this indicates that the low level of CTC-EC interactions in UF can be attributed to the abundance of the protective GCX

We investigated the effects of Neur-induced GCX degradation on the attachment of CTCs to the endothelium. Based on a dose response experiment in static conditions (Fig. S4) and a confirmatory experiment in UF experiments, it was determined that a Neur concentration of 15mU/mL was the best concentration of enzyme for GCX degradation while keeping HUVEC layers intact, stable, and firmly attached to their substrate (Fig.4A and 4F) so that they would be able to withstand the force of UF conditions. In static conditions, this 15mU/mL concentration was effective to statistically significantly reduce the coverage of the ECs by the WGA-labeled GCX, which is primarily the SA component of the GCX (Fig. S4B and S4F). In static conditions 15 mU/mL of Neur did not affect WGA-labeled GCX thickness (Fig. S4G). However, the presence of 15 mU/mL of Neur in UF conditions, compared to untreated UF conditions, was effective to reduce WGA-labeled GCX with respect to both its coverage of the ECs and its thickness on top of the ECs (Fig. 4B and 4G). In UF without Neur, the normalized GCX coverage was 1.00±1.11 (Fig. 4B and 4K) and coverage for GCX after supplementing UF with 15mU/mL of enzyme was 0.21±0.01 (Fig. 4G and 4K). The corresponding normalized thickness of GCX with UF in the absence of Neur was at 1.00±0.14 (Fig. 4B orthogonal view and Fig. 4L). In UF with Neur the normalized GCX thickness was at 0.37±0.01(Fig.4G orthogonal view and Fig. 4L). These results indicate the fact that, in UF conditions, the presence of GCX degrading enzyme is very detrimental to the health of GCX.

The presence of 15 mU/mL of Neur in UF conditions not only degraded the GCX but also decreased E-selectin coverage. It was found that E-selectin is more significantly expressed in isolated UF conditions than in UF conditions where Neur is present at a concentration of 15mU/mL. Exposure of ECs to isolation UF resulted in E-selectin coverage at a normalized level of 1.00±0.23 (Fig. 4C and 4M). After the addition of Neur to UF, we saw a statistically significant reduction of E-selectin coverage to 0.21±0.01(Fig. 4H and 4M), an approximate 80 percent decrease in the coverage of E-selectin. Since Neur treatment degraded GCX while also removing E-selectin, it was not clear whether we would observe increased CTC-EC interactions due to GCX loss or whether we would find unchanged or decreased CTC-EC interactions due to E-selectin deficiency.

As previously mentioned, UF conditions in the absence of Neur yielded 4T1 cells to attach to HUVEC at a normalized count of 1.00±0.13 (Fig. 4D and 4N). Adding 15mU/mL of Neur to UF resulted in a statistically significant increase in 4T1-to-HUVEC attachment to 2.60±0.34 (Fig. 4I and 4N). We observed a statistically significant increase in initiated migration of 4T1 cells through the endothelium, when conditions of UF with Neur were compared to conditions of isolated UF. Specifically, a normalized 1.00±0.24 (Fig. 4D and 4P) count of 4T1 cells initiated migrated through samples of HUVEC layers which had been exposed to only UF conditions, while a normalized 6.50±1.72 (Fig. 4I and 4P) count of 4T1

cells initiated migrated through the endothelium that had been exposed to UF and 15mU/mL of Neur simultaneously. Clustering of 4T1 cells was 1.00±0.21 (Fig. 4D and 4O) for UF-only conditions and the clustering level increased to 1.90±0.59 (Fig. 4I and 4O) in conditions of UF with Neur, which was statistically insignificant.

When we matched the endothelium species with the CTC species, by utilizing MCF7 CTCs in place of 4T1 CTCs, we observed a normalized number of MCF7-to-HUVEC attachments of 1.00±0.19 (Fig. 4E and 4N). Adding 15mU/mL of Neur to the UF condition resulted in a statistically significant increase in the attachment of MCF7 cells to HUVEC, at the normalized level of 3.8±0.55 (Fig. 4J and 4N). We also observed a statistically significant change in MCF7 cell clustering. In isolated UF conditions, the normalized value of MCF7 clustering was at 1.00±0.22 (Fig. 4E and 4O). After addition of Neur to the UF environment, clustering significantly increased to the normalized value of 6.10±1.48 (Fig. 4J and 4O). There was also a change in the level of initiated migration of MCF7 cells across layers of ECs. Without Neur enzyme treatment, UF stimuli led to the initiated migration of MCF7 cells at a normalized level of 1.00 ±0.24 (Fig. 4E and 4P). With Neur enzyme treatment, we observed a statically significant increase in MCF7 initiated trans-endothelial migration to a normalized level of 3.10±0.25 (Fig. 4J and 4P). The 4T1 and MCF7 CTC attachment, clustering, and migration results were consistent with what would be expected due to GCX loss and inconsistent with what would be expected due to E-selectin deficiency.

3.4 In an in vivo setting, the presence of GCX-degrading Neur in the circulating blood results in an increase in CTC homing to the lung, an organ where secondary tumors are commonly found

This *in vivo* experiment was carried out in Balb/c mice to confirm our observed *in vitro* findings. We confirmed that the coverage and thickness of GCX lining the vascular walls of the Balb/c mice were statistically significantly decreased after treating Balb/c mice with 5U/mL of Neur. For non-treated mice the normalized expression of GCX coverage was at 1.00± 0.01 (Fig. 5A and 5C) while the GCX coverage for Neur-treated mice was 0.85±0.04 (Fig. 5B and 5C). In the case of GCX thickness, the normalized data for non-treated mice was 1.00±0.09 (Fig. 5A and 5D) and for enzyme-treated samples the normalized thickness was 0.71±0.03 (Fig. 5B and 5D). We also confirmed that the endothelium integrity was maintained in both control and Neur-treated mice by staining for the following EC markers: eNOS, E-selectin, PECAM-1, and ZO-1 (Fig. 6A through 6H). Since we were interested in comparing GCX levels to E-selectin levels, we quantified E-selectin coverage. The normalized level of E-selectin in untreated mice was 1.00±0.57 (Fig. 6C and 6I) and for enzyme-treated mice the normalized E-selectin level was 0.60±0.28 (Fig. 6D and 6I). The E-selectin levels are not statistically significantly different.

4T1 CTCs were introduced into the blood of Balb/c mice that were not treated or those that were treated with 5U/mL of Neur. With DiFC, the 4T1 cells were observed to significantly clear the arterial and venous blood flow over the course of 1 hour (Fig. 7A and 7B). At 10, 30, and 60 minutes after 4T1 cells were introduced, DiFC detected circulating 4T1 at a rate of 8.51, 3.69, and 3.1 cells per minute in the Balb/C arteries and the veins (Fig. 7A and 7B). The decreasing rate, which served as an indicator of substantial 4T1 clearance from the

blood stream, was expected to correspond to 4T1 attachment to the vascular wall or clearance from the blood stream altogether. Therefore, at the 60-minute time point we determined if 4T1 cells were attached by examining the Balb/c lungs. We found that for Balb/c mice with intact GCX (lack of Neur treatment), the normalized number of 4T1 attachment to the vessel walls in the lungs was 1.00±0.14 (Fig. 7C and 7E). We observed a statistically significant 2.2-fold increase in the attachment of 4T1 cells to the GCX-deficient (due to Neur treatment) vessel walls of the Balb/c lungs (Fig. 7D and 7E).

4. DISCUSSION

In this study, we demonstrated the importance of EC GCX regulation of cancer cell attachment to the endothelium. We also showed that the increase in cancer cell attachment to the endothelium, which results from decreased GCX expression, can more preferentially occur in areas of the vasculature with DF patterns, in comparison with UF areas. Activation of the adhesion molecule E-selectin in different flow conditions was not the primary contributor to increased cancer attachment to the endothelium. On the other hand, the absence of a healthy, robust GCX appeared to be extensively and primarily involved in the enhancement of cancer cell attachment to the endothelium. Our results provide new insights into the possible pathways leading to secondary tumor formations during cancer progression.

The mechanisms underlying secondary tumor formation remain an active area of ongoing research and recent studies suggest that interaction between CTCs and the endothelium is an important driver of cancer cell migration from the primary tumor site to secondary tumor sites [48, 49]. Until now, there have been few studies conducted to examine the role of the endothelial GCX in mediating these CTC-to-endothelium intercellular interactions [50]. Here, we have provided evidence that suggests that the GCX is pivotal in mediating CTC-EC interactions leading to secondary tumor formation.

We began our study by using a previously developed parallel plate flow chamber model [24] that recreates flow patterns (UF and DF) similar to what is observed *in vivo* [51, 52]. We tested the hypothesis that DF regions of the vascular system could enhance the attachment of cancer cells to the endothelium. After introducing DF and UF conditions to HUVEC, we co-incubated HUVEC monolayers with either 4T1 or MCF7 breast cancer cells. As predicted, we observed a significant increase in the attachment and immobilization of 4T1 or MCF7 breast cancer cells to the endothelium in DF regions compared with UF regions (Fig. 2D, 2E and 2F). Considering the fact that 4T1 cells originate from mice and MCF7 cells originate from humans, our finding shows that preferential CTC attachment to the DF area is not species specific. However, it is important to mention that we observed a higher rate of MCF7 attachment to HUVEC compared to 4T1 attachment to HUVEC, indicating that proper species match is very important. Any other cancer cell type that has affinity to receptors on the endothelial surface should produce the same attachment results. This confirms an earlier report by Yamaguchi *et al.,* that cancer cells are more likely to adhere to bifurcated regions in blood vessels where DF exits, and less likely to adhere in other locations of the vascular tree where UF exist [53].

Breast cancer cell clustering has been reported to have a significant effect on the metastatic potential of the tumor [54–56]. Specifically, Nicola *et al* reported that CTC clusters, although rare to find in blood flow, have a 23-fold to 50-fold increased likelihood of resulting in metastasis [54]. Guided by the prior reports, in the present study we investigated the potential for DF patterns to regulate cancer cell clustering that could enhance secondary tumor formation. We observed substantial increases in the rate of clustering of 4T1 and MCF7 breast cancer cells (Fig. 2D, 2E and 2G) in regions of DF, compared to regions of UF. It was previously suggested that metastatic cancer cells are more likely to break away from the primary tumor in clusters and travel in groupings to the secondary tumor site [54]. It was also suggested that metastatic cancer cells are less likely to break away from the primary tumor as individual cells, a situation in which cells would form clusters somewhere along the vessel pathway or at the vessel wall where the secondary tumor will form [54]. From our study, we cannot determine which situation is the case. However, if the former is true, then our results show that clustered CTCs prefer to land at sites of DF while individual CTCs prefer to land at sites of UF. If the latter is true, then our results show that CTCs more readily aggregate in the presence of DF patterns than they do in the presence of UF patterns.

CTC migration from the apical side of the endothelium, across the endothelium, and into the underlying tissue are the last steps in the process of secondary tumor initiation [57, 58]. Therefore, we investigated the potential of attached 4T1 or MCF7 breast cancer cells to migrate through the endothelium after successful attachment to the endothelium. Both cell types exhibited the same trend of higher transendothelial migration in DF versus UF conditions. 4T1 breast cancer cells were observed to initially migrate across the endothelium at a statistically significant high rate in the DF region, in comparison to the rate of initial migration in UF areas (Fig. 2H). For MCF7 cells, on the other hand, exhibited statistically nonsignificant increase in the rate of initial migration across the endothelium in DF regions compared to UF regions (Fig. 2H). This may be due to 4T1 breast cancer cells possessing a higher degree of activated invadopodia than MCF7 breast cancer cells [59, 60].

We sought to identify a mechanism that could enable DF-induced CTC interactions with ECs. It has been reported that DF initiates EC dysfunction [52], which leads to the progression of disease [15]. Previous reports rarely consider that DF is a contributing factor to GCX degradation [61–64]. On average, components of the GCX in both humans and animals degrade and regenerate on a daily basis and in a balanced manner [65, 66]. However, as our group and others [24, 67–69] have highlighted, DF has a negative effect on the endothelial GCX [17, 70]. Based on this prior research, we believe that degraded GCX could play a direct role in regulating DF-induced CTC interactions with ECs. Therefore, we characterized the expression of HUVEC GCX in DF and UF regions of the flow chamber (Fig. 3A, 3B, and 3C). Compared with UF conditions, we observed a more than 2-fold decrease in both the coverage and thickness of GCX in DF regions (Fig. 3B, 3F, and 3G). This is similar to what we previously observed in rat ECs [24], suggesting that the effects of DF on GCX is consistent across EC types from different species. It is clear from our observations that GCX degradation outweighs GCX regeneration in the DF regions of the vascular system (Fig. 3A–3C, 3F, and 3G). As reported by numerous studies [17, 26, 71, 72], including the present investigation, UF is protective of the endothelium and results in a healthy, robust GCX [25, 73, 74].

In UF regions, healthy GCX can shield receptors on the endothelium surface and block binding of CTC to the endothelium. Degraded GCX in DF regions of the blood vessels could expose receptor sites on the surface of the endothelium for easy binding of CTCs to the endothelium surface (Fig. 3) [75, 76] because these adhesion molecules lie beneath the endothelial GCX surface and are attached to the cell membrane. Another plausible explanation is that DF could be pro-inflammatory and could enhance the expression of adhesion receptors. Once the GCX layer is removed and the adhesion molecule receptor sites are exposed in DF, or once adhesion receptors are overexpressed in DF, CTC-to-EC intercellular interactions can become enhanced. It follows that CTCs would likely prefer to undergo transendothelial migration at DF regions of the vasculature, due to the proven decrease in GCX expression.

We examined whether the attachment of cancer cells to the endothelium in either DF or UF was due to degraded endothelial GCX or overexpressed endothelial surface adhesion receptors, namely activated E-selectin although there are other adhesion molecules that should be explored in future studies. It was important for us to verify whether decreased GCX expression in DF regions directly causes increased cell attachment, clustering and migration, or whether CTC-to-EC intercellular interactions are caused by E-selectin activity in DF conditions. To this end, we first investigated the coverage of ECs by E-selectin in the different flow conditions. We did not observe any statistically significant difference between E-selectin coverage in DF and UF conditions (Fig. 3D, 3E, and 3H). Our E-selectin findings are unexpected based on prior research publications. For example, Huang et al, showed that UF downregulates E-selectin coverage by HUVEC, in a time-dependent manner and to protect the endothelium against chronic inflammation [77]. This prior study and others, unlike ours, compared E-selectin coverage in static versus UF conditions and did not compare DF versus UF conditions. In addition, our HUVEC exposure time was enough to disrupt GCX expression in the DF region but not enough to have resulted in a significant expression of E-selectin.

We next attempted to investigate the effects of GCX degradation in the presence of stable E-selectin coverage. It is possible to achieve systemic GCX knockdown by pro-inflammatory cytokines or enzymes that increase reactive oxygen species and matrix metalloproteases activities [61]. These agents are naturally released in certain disease settings including atherosclerosis, ischemia/reperfusion and cancer [17, 64, 78, 79]. In our study, we mimicked systemic degradation of GCX *in vitro* by adding 15 mU/mL of Neur to UF conditions, as previously described above, and we characterized the expression of GCX (Fig. 4G). We observed that the enzyme significantly decreased both the coverage and thickness of GCX in UF conditions (Fig. 4B, 4G, 4K, and 4L). This result is similar to the degradation of the endothelial GCX that is a reported effect of systemic enzyme or cytokine release in disease [80–82]. After successful degradation of GCX in UF settings, we would expect a high level of interaction between CTCs and ECs. However, when we investigated E-selectin expression we unexpectedly found that adding 15 mU/mL of Neur to UF destabilized and decreased the coverage of E-selectin (Fig. 4C, 4H, and 4M). Although, this Neur-induced E-selectin decrease could hinder CTC-to-EC interactions, we found instead that Neur increased 4T1 and MCF7 breast cancer cell attachment, clustering and migration to ECs to levels that were

similar to what we found due to DF stimulation. This increase in CTC-to-EC interactions can only be attributed to GCX degradation and not to E-selectin degradation.

We aimed to confirm our cell culture results with animal data that shows enhancement of CTC homing in DF conditions and due to GCX degradation. Towards this end, we first relied on a parallel experiment conducted by members of our research group using a technique similar to the aforementioned DiFC technique, called computer vision *in vivo* flow cytometry (CV-IVFC; Markovic et al. [46, 83, 84]). In that experiment, a video-rate fluorescence macroscope was used to monitor in real time the movement of CTCs in the vessels within the transparent 250–300 μm thick ears of nude mice [46, 83, 84]. For the purpose of the present study, we have re-analyzed the video data from that experiment (Fig. S8A–S8D). We have quantified the speeds of CTCs in motion (Fig. S8C). We found that the average speed of CTC motion in the ear of nude mice was reduced in the branched (DF) vessel sections in comparison with the straight (UF) vessel sections (Fig. S8C). This attenuated motion of CTCs increases the possibility of interactions and formation of firm adhesions between CTCs and ECs. Quantifying the number of CTCs attached (Fig. S8D) to the walls of branched (DF) vessel sections versus straight (UF) vessel sections within the ear of the nude mice, we observed a higher average number of CTCs attached in branched (DF) vessel sections as compared to straight (UF) vessel sections (Fig. S8D). The CTC speed and attachment results shown in Figs. S8C and S8D are, again, from parallel experiments. Although a decrease in speed and increase in attachment was observed on average for these data, the difference was not statistically significant in part due to the relatively low number of attachment events observed in those studies. We plan to address this in the future by increasing the sample size. Secondly, as shown in Figs. S8E and S8F, we relied on another *in vivo* study conducted by our research group, which confirms the link between DF flow conditions (induced by partial ligation of the carotid arteries) and degradation of GCX coverage and thickness, as compared to a link between UF conditions and robust GCX (Mitra et al. [24] and Cheng et al. [Ann Biomed Eng, 2020, in press]). Our previously conducted study of GCX in DF conditions *in vivo* suggests that GCX is indeed degraded in the branched (DF) areas of the mouse ear vessels, enabling the endothelium covered vessel walls to recruit CTCs, as indicated by reduction in CTC speed and the increased CTC attachment that we see.

To further confirm the cell culture results, in the present study we treated Balb/C mice with 5 U/mL of Neur. We quantified the effects of the enzyme on the endothelium of the abdominal aortas of treated and untreated mice. We observed on this endothelium a significant reduction in the expression of GCX (Fig. 5). We also confirmed that only GCX on the endothelial layer was affected by Neur enzyme and that the endothelium was not denuded, by the localizing four EC markers including E-selectin (Fig. 6A–6H). Quantification of E-selectin revealed that its expression level was not altered by Neur (Fig. 6I). Lastly, we investigated the effect of Neur on 4T1 breast cancer cell attachment to mouse lungs. We observed a significant 2-fold increase in the attachment of 4T1 breast cancer cells to the lungs of Neur-treated mice in comparison with untreated samples (Fig. 7C–7E). These results are consistent with a prior study by Rai *et al*, in which they observed a significant increase in the attachment of lung cancer cells to the endothelial monolayers after the degradation of the WGA-labeled GCX [1].

In summary, our data indicate that DF areas of the vasculature could represent points of entry for CTCs into tissue sites where they can form secondary tumors and, thereby, advance cancer progression. In addition, DF-induced degradation of endothelial GCX, specifically the SA component, plays a critical role in regulating the interactions of CTCs with the endothelium.

Supplementary Material

Refer to Web version on PubMed Central for supplementary material.

Other Acknowledgements

We thank Northeastern University Biology core facility and Prof Heather Clark for permitting us to use their confocal microscopes.

Sources of Funding: This work was funded by the National Institutes of Health (K01 HL125499 awarded to E. Ebong and 1R01HL124315-01A1 awarded to M. Niedre), the American Heart Association (18PRE33960461 awarded to I. Harding), the National Science Foundation (DGE-1451070 awarded to S. Mensah; CMMI- 1846962 awarded to E. Ebong), and Northeastern University (startup funds and Tier 1 Provost Grant awarded to E. Ebong; Engineering Dean's Fellowship awarded to I. Harding). The funders had no role in data or information collection and analysis, decision to publish, or preparation of the manuscript.

ABBREVIATIONS

4T1	Stage IV Metastatic Breast Cancer Cells
BSA	Bovine Serum Albumin
CTC	Circulating Tumor Cells
DAPI	4‘‘6-diamidino-2-phenylindole
DMEM	Dulbecco's Modified Eagle Medium
DF	Disturbed Flow
ECs	Endothelial Cells
EMEM	Eagle's Minimum Essential Medium
eNOS	Endothelial nitric oxide synthase
FBS	Fetal Bovine Serum
GCX	Endothelial Glycocalyx
MCF7	Human breast cancer cells
Neur	Neuraminidase
PECAM-1	Platelet endothelial cell adhesion molecule-1
PBS	Phosphate Buffered Saline
RT	Room Temperature

SA	Sialic Acid
TNF-α	Tumor Necrosis Factor- α
UF	Uniform Flow
VEGF	Vascular Endothelial Growth Factor
WGA	Wheat Germ Agglutinin Lectin
HUVEC	Human Umbilical Vein Endothelial Cells

REFERENCES

1. Rai S, Nejadhamzeeigilani Z, Gutowski NJ, and Whatmore JL, Loss of the endothelial glycocalyx is associated with increased E-selectin mediated adhesion of lung tumour cells to the brain microvascular endothelium. J Exp Clin Cancer Res, 2015 34: p. 105. [PubMed: 26407999]
2. De Souza LM, Robertson BM, and Robertson GP, Future of circulating tumor cells in the melanoma clinical and research laboratory settings. Cancer Lett, 2017 392: p. 60–70. [PubMed: 28163189]
3. Goel S, Duda DG, Xu L, Munn LL, Boucher Y, Fukumura D, and Jain RK, Normalization of the vasculature for treatment of cancer and other diseases. Physiol Rev, 2011 91(3): p. 1071–121. [PubMed: 21742796]
4. Hashizume H, Baluk P, Morikawa S, McLean JW, Thurston G, Roberge S, Jain RK, and McDonald DM, Openings between defective endothelial cells explain tumor vessel leakiness. Am J Pathol, 2000 156(4): p. 1363–80. [PubMed: 10751361]
5. Cegan M, Kobierzycki C, Kolostova K, Kiss I, Bobek V, and Grill R, Circulating tumor cells in urological cancers. Folia Histochem Cytobiol, 2017 55(3): p. 107–113. [PubMed: 28994093]
6. Zhou J, Ma X, Bi F, and Liu M, Clinical significance of circulating tumor cells in gastric cancer patients. Oncotarget, 2017 8(15): p. 25713–25720. [PubMed: 28147337]
7. Lee AM, Tormoen GW, Kanso E, McCarty OJ, and Newton PK, Modeling and simulation of procoagulant circulating tumor cells in flow. Front Oncol, 2012 2: p. 108. [PubMed: 23050240]
8. Takeishi N, Imai Y, Ishida S, Omori T, Kamm RD, and Ishikawa T, Cell adhesion during bullet motion in capillaries. Am J Physiol Heart Circ Physiol, 2016 311(2): p. H395–403. [PubMed: 27261363]
9. Sullivan TM, Ainsworth SD, Langan EM, Taylor S, Snyder B, Cull D, Youkey J, and Laberge M, Effect of endovascular stent strut geometry on vascular injury, myointimal hyperplasia, and restenosis. J Vasc Surg, 2002 36(1): p. 143–9. [PubMed: 12096272]
10. Townsley MI, Structure and composition of pulmonary arteries, capillaries, and veins. Compr Physiol, 2012 2(1): p. 675–709. [PubMed: 23606929]
11. Kline TL, Zamir M, and Ritman EL, Relating function to branching geometry: a micro-CT study of the hepatic artery, portal vein, and biliary tree. Cells Tissues Organs, 2011 194(5): p. 431–42. [PubMed: 21494011]
12. Disibio G and French SW, Metastatic patterns of cancers: results from a large autopsy study. Arch Pathol Lab Med, 2008 132(6): p. 931–9. [PubMed: 18517275]
13. Guo P, Cai B, Lei M, Liu Y, and Fu BM, Differential arrest and adhesion of tumor cells and microbeads in the microvasculature. Biomech Model Mechanobiol, 2014 13(3): p. 537–50. [PubMed: 23880911]
14. Nakajima H and Mochizuki N, Flow pattern-dependent endothelial cell responses through transcriptional regulation. Cell Cycle, 2017 16(20): p. 1893–1901. [PubMed: 28820314]
15. Chiu JJ and Chien S, Effects of disturbed flow on vascular endothelium: pathophysiological basis and clinical perspectives. Physiol Rev, 2011 91(1): p. 327–87. [PubMed: 21248169]
16. Chien S, Effects of disturbed flow on endothelial cells. Ann Biomed Eng, 2008 36(4): p. 554–62. [PubMed: 18172767]

17. Cancel LM, Ebong EE, Mensah S, Hirschberg C, and Tarbell JM, Endothelial glycocalyx, apoptosis and inflammation in an atherosclerotic mouse model. Atherosclerosis, 2016 252: p. 136–146. [PubMed: 27529818]
18. Clark AG and Vignjevic DM, Modes of cancer cell invasion and the role of the microenvironment. Curr Opin Cell Biol, 2015 36: p. 13–22. [PubMed: 26183445]
19. Brabletz T, Jung A, Reu S, Porzner M, Hlubek F, Kunz-Schughart LA, Knuechel R, and Kirchner T, Variable beta-catenin expression in colorectal cancers indicates tumor progression driven by the tumor environment. Proc Natl Acad Sci U S A, 2001 98(18): p. 10356–61. [PubMed: 11526241]
20. Prall F, Tumour budding in colorectal carcinoma. Histopathology, 2007 50(1): p. 151–62. [PubMed: 17204028]
21. Kundra P and Goswami S, Endothelial glycocalyx: Role in body fluid homeostasis and fluid management. Indian J Anaesth, 2019 63(1): p. 6–14. [PubMed: 30745606]
22. Cheng MJ, Bal NN, Prabakaran P, Kumar R, Webster TJ, Sridhar S, and Ebong EE, Ultrasmall gold nanorods: synthesis and glycocalyx-related permeability in human endothelial cells. Int J Nanomedicine, 2019 14: p. 319–333. [PubMed: 30697044]
23. Zeng Y, Adamson RH, Curry FR, and Tarbell JM, Sphingosine-1-phosphate protects endothelial glycocalyx by inhibiting syndecan-1 shedding. Am J Physiol Heart Circ Physiol, 2014 306(3): p. H363–72. [PubMed: 24285115]
24. Harding IC, Mitra R, Mensah SA, Herman IM, and Ebong EE, Pro-atherosclerotic disturbed flow disrupts caveolin-1 expression, localization, and function via glycocalyx degradation. J Transl Med, 2018 16(1): p. 364. [PubMed: 30563532]
25. Gouverneur M, Spaan JA, Pannekoek H, Fontijn RD, and Vink H, Fluid shear stress stimulates incorporation of hyaluronan into endothelial cell glycocalyx. Am J Physiol Heart Circ Physiol, 2006 290(1): p. H458–2. [PubMed: 16126814]
26. Koo A, Dewey CF Jr., and Garcia-Cardena G, Hemodynamic shear stress characteristic of atherosclerosis-resistant regions promotes glycocalyx formation in cultured endothelial cells. Am J Physiol Cell Physiol, 2013 304(2): p. C137–46. [PubMed: 23114962]
27. Harding IC, Mitra R, Mensah SA, Nersesyan A, Bal NN, and Ebong EE, Endothelial barrier reinforcement relies on flow-regulated glycocalyx, a potential therapeutic target. Biorheology, 2019.
28. Nishitani S, Maekawa Y, and Sakata T, Understanding the Molecular Structure of the Sialic Acid-Phenylboronic Acid Complex by using a Combined NMR Spectroscopy and DFT Study: Toward Sialic Acid Detection at Cell Membranes. ChemistryOpen, 2018 7(7): p. 513–519. [PubMed: 30003005]
29. Mensah SA, Harding IC, Zhang M, Jaeggli MP, Torchilin VP, Niedre MJ, and Ebong EEJAJ, Metastatic Cancer Cell Attachment to Endothelium is Promoted by Endothelial Glycocalyx Sialic Acid Degradation.
30. Okegawa T, Pong RC, Li Y, and Hsieh JT, The role of cell adhesion molecule in cancer progression and its application in cancer therapy. Acta Biochim Pol, 2004 51(2): p. 445–57. [PubMed: 15218541]
31. Kobayashi H, Boelte KC, and Lin PC, Endothelial cell adhesion molecules and cancer progression. Curr Med Chem, 2007 14(4): p. 377–86. [PubMed: 17305540]
32. Barthel SR, Gavino JD, Descheny L, and Dimitroff CJ, Targeting selectins and selectin ligands in inflammation and cancer. Expert Opin Ther Targets, 2007 11(11): p. 1473–91. [PubMed: 18028011]
33. Ebong EE, Macaluso FP, Spray DC, and Tarbell JM, Imaging the endothelial glycocalyx in vitro by rapid freezing/freeze substitution transmission electron microscopy. Arterioscler Thromb Vasc Biol, 2011 31(8): p. 1908–15. [PubMed: 21474821]
34. Sarangapani KK, Marshall BT, McEver RP, and Zhu C, Molecular stiffness of selectins. J Biol Chem, 2011 286(11): p. 9567–76. [PubMed: 21216951]
35. Huang J, Chen J, Chesla SE, Yago T, Mehta P, McEver RP, Zhu C, and Long M, Quantifying the effects of molecular orientation and length on two-dimensional receptor-ligand binding kinetics. J Biol Chem, 2004 279(43): p. 44915–23. [PubMed: 15299021]

36. Chappell D, Hofmann-Kiefer K, Jacob M, Rehm M, Briegel J, Welsch U, Conzen P, and Becker BF, TNF-alpha induced shedding of the endothelial glycocalyx is prevented by hydrocortisone and antithrombin. Basic Res Cardiol, 2009 104(1): p. 78–89. [PubMed: 18836678]
37. Li YT, Goswami D, Follmer M, Artz A, Pacheco-Blanco M, and Vestweber D, Blood flow guides sequential support of neutrophil arrest and diapedesis by PILR-beta1 and PILR-alpha. Elife, 2019 8.
38. Buchanan CF, Verbridge SS, Vlachos PP, and Rylander MN, Flow shear stress regulates endothelial barrier function and expression of angiogenic factors in a 3D microfluidic tumor vascular model. Cell Adh Migr, 2014 8(5): p. 517–24. [PubMed: 25482628]
39. Sung BH, Kim SH, Yeo MG, Kim JK, and Song WK, Human soluble E-selectin immunoadhesin inhibits leukemic monocyte adhesion to endothelial cells. Cell Biochem Funct, 2007 25(5): p. 585–9. [PubMed: 16892455]
40. Reitsma S, Slaaf DW, Vink H, van Zandvoort MA, and oude Egbrink MG, The endothelial glycocalyx: composition, functions, and visualization. Pflugers Arch, 2007 454(3): p. 345–59. [PubMed: 17256154]
41. Singh A, Satchell SC, Neal CR, McKenzie EA, Tooke JE, and Mathieson PW, Glomerular endothelial glycocalyx constitutes a barrier to protein permeability. J Am Soc Nephrol, 2007 18(11): p. 2885–93. [PubMed: 17942961]
42. Schmidt EP, Yang Y, Janssen WJ, Gandjeva A, Perez MJ, Barthel L, Zemans RL, Bowman JC, Koyanagi DE, Yunt ZX, Smith LP, Cheng SS, Overdier KH, Thompson KR, Geraci MW, Douglas IS, Pearse DB, and Tuder RM, The pulmonary endothelial glycocalyx regulates neutrophil adhesion and lung injury during experimental sepsis. Nat Med, 2012 18(8): p. 1217–23. [PubMed: 22820644]
43. Sukhikh GT, Ziganshina MM, Nizyaeva NV, Kulikova GV, Volkova JS, Yarotskaya EL, Kan NE, Shchyogolev AI, and Tyutyunnik VL, Differences of glycocalyx composition in the structural elements of placenta in preeclampsia. Placenta, 2016 43: p. 69–76. [PubMed: 27324102]
44. Pera V, Tan X, Runnels J, Sardesai N, Lin CP, and Niedre M, Diffuse fluorescence fiber probe for in vivo detection of circulating cells. J Biomed Opt, 2017 22(3): p. 37004. [PubMed: 28290598]
45. Tan X, Patil R, Bartosik P, Runnels JM, Lin CP, and Niedre M, In Vivo Flow Cytometry of Extremely Rare Circulating Cells. Sci Rep, 2019 9(1): p. 3366. [PubMed: 30833671]
46. Hartmann C, Patil R, Lin CP, and Niedre MJ, Fluorescence detection, enumeration and characterization of single circulating cells in vivo: technology, applications and future prospects. Phys Med Biol, 2017.
47. Patil R, Tan X, Bartosik P, Detappe A, Runnels JM, Ghobrial I, Lin CP, and Niedre M, Fluorescence monitoring of rare circulating tumor cell and cluster dissemination in a multiple myeloma xenograft model in vivo. J Biomed Opt, 2019 24(8): p. 1–11.
48. Fu BM, Tumor Metastasis in the Microcirculation. Adv Exp Med Biol, 2018 1097: p. 201–218. [PubMed: 30315547]
49. Stojak M, Kaczara P, Motterlini R, and Chlopicki S, Modulation of cellular bioenergetics by CO-releasing molecules and NO-donors inhibits the interaction of cancer cells with human lung microvascular endothelial cells. Pharmacol Res, 2018 136: p. 160–171. [PubMed: 30196104]
50. Fan J and Fu BM, Quantification of Malignant Breast Cancer Cell MDA-MB-231 Transmigration Across Brain and Lung Microvascular Endothelium. Ann Biomed Eng, 2016 44(7): p. 2189–201. [PubMed: 26603751]
51. Charoenphol P, Onyskiw PJ, Carrasco-Teja M, and Eniola-Adefeso O, Particle-cell dynamics in human blood flow: implications for vascular-targeted drug delivery. J Biomech, 2012 45(16): p. 2822–8. [PubMed: 23010218]
52. Rocha HNM, Garcia VP, Batista GMS, Silva GM, Mattos JD, Campos MO, Nobrega ACL, Fernandes IA, and Rocha NG, Disturbed blood flow induces endothelial apoptosis without mobilizing repair mechanisms in hypertension. Life Sci, 2018 209: p. 103–110. [PubMed: 30076919]
53. Ishikawa T, Fujiwara H, Matsuki N, Yoshimoto T, Imai Y, Ueno H, and Yamaguchi T, Asymmetry of blood flow and cancer cell adhesion in a microchannel with symmetric bifurcation and confluence. Biomed Microdevices, 2011 13(1): p. 159–67. [PubMed: 20960063]

54. Aceto N, Bardia A, Miyamoto DT, Donaldson MC, Wittner BS, Spencer JA, Yu M, Pely A, Engstrom A, Zhu H, Brannigan BW, Kapur R, Stott SL, Shioda T, Ramaswamy S, Ting DT, Lin CP, Toner M, Haber DA, and Maheswaran S, Circulating tumor cell clusters are oligoclonal precursors of breast cancer metastasis. Cell, 2014 158(5): p. 1110–1122. [PubMed: 25171411]
55. Lambert AW, Pattabiraman DR, and Weinberg RA, Emerging Biological Principles of Metastasis. Cell, 2017 168(4): p. 670–691. [PubMed: 28187288]
56. Gava F, Rigal L, Mondesert O, Pesce E, Ducommun B, and Lobjois V, Gap junctions contribute to anchorage-independent clustering of breast cancer cells. BMC Cancer, 2018 18(1): p. 221. [PubMed: 29482519]
57. Asaad A, Abdalla AS, Idaewor P, Jayasooryia B, Yates V, Eldruki S, and English J, Breast Metastasis as a Presentation of Malignant Melanoma. Chirurgia (Bucur), 2018 113(5): p. 712–718. [PubMed: 30383998]
58. Manni A, Washington S, Hu X, Griffith JW, Bruggeman R, Demers LM, Mauger D, and Verderame MF, Effects of polyamine synthesis inhibitors on primary tumor features and metastatic capacity of human breast cancer cells. Clin Exp Metastasis, 2005 22(3): p. 255–63. [PubMed: 16158253]
59. Yin M, Ma W, and An L, Cortactin in cancer cell migration and invasion. Oncotarget, 2017 8(50): p. 88232–88243. [PubMed: 29152154]
60. Friedl P and Wolf K, Tumour-cell invasion and migration: diversity and escape mechanisms. Nat Rev Cancer, 2003 3(5): p. 362–74. [PubMed: 12724734]
61. Wang L, Huang X, Kong G, Xu H, Li J, Hao D, Wang T, Han S, Han C, Sun Y, Liu X, and Wang X, Ulinastatin attenuates pulmonary endothelial glycocalyx damage and inhibits endothelial heparanase activity in LPS-induced ARDS. Biochem Biophys Res Commun, 2016 478(2): p. 669–75. [PubMed: 27498004]
62. Burke-Gaffney A and Evans TW, Lest we forget the endothelial glycocalyx in sepsis. Crit Care, 2012 16(2): p. 121.
63. Johansson PI, Stensballe J, Rasmussen LS, and Ostrowski SR, A high admission syndecan-1 level, a marker of endothelial glycocalyx degradation, is associated with inflammation, protein C depletion, fibrinolysis, and increased mortality in trauma patients. Ann Surg, 2011 254(2): p. 194–200. [PubMed: 21772125]
64. Rehm M, Bruegger D, Christ F, Conzen P, Thiel M, Jacob M, Chappell D, Stoeckelhuber M, Welsch U, Reichart B, Peter K, and Becker BF, Shedding of the endothelial glycocalyx in patients undergoing major vascular surgery with global and regional ischemia. Circulation, 2007 116(17): p. 1896–906. [PubMed: 17923576]
65. Song JW, Zullo JA, Liveris D, Dragovich M, Zhang XF, and Goligorsky MS, Therapeutic Restoration of Endothelial Glycocalyx in Sepsis. J Pharmacol Exp Ther, 2017 361(1): p. 115–121. [PubMed: 28167639]
66. Fraser JR, Laurent TC, and Laurent UB, Hyaluronan: its nature, distribution, functions and turnover. J Intern Med, 1997 242(1): p. 27–33. [PubMed: 9260563]
67. Mitra R, Qiao J, Madhavan S, O'Neil GL, Ritchie B, Kulkarni P, Sridhar S, van de Ven AL, Kemmerling EMC, Ferris C, Hamilton JA, and Ebong EE, The comparative effects of high fat diet or disturbed blood flow on glycocalyx integrity and vascular inflammation. Transl Med Commun, 2018 3.
68. Korshunov VA and Berk BC, Flow-induced vascular remodeling in the mouse: a model for carotid intima-media thickening. Arterioscler Thromb Vasc Biol, 2003 23(12): p. 2185–91. [PubMed: 14576075]
69. Nam D, Ni CW, Rezvan A, Suo J, Budzyn K, Llanos A, Harrison D, Giddens D, and Jo H, Partial carotid ligation is a model of acutely induced disturbed flow, leading to rapid endothelial dysfunction and atherosclerosis. Am J Physiol Heart Circ Physiol, 2009 297(4): p. H1535–43. [PubMed: 19684185]
70. Cooper S, Emmott A, McDonald KK, Campeau MA, and Leask RL, Increased MMP activity in curved geometries disrupts the endothelial cell glycocalyx creating a proinflammatory environment. PLoS One, 2018 13(8): p. e0202526. [PubMed: 30138400]

71. Giantsos-Adams KM, Koo AJ, Song S, Sakai J, Sankaran J, Shin JH, Garcia-Cardena G, and Dewey CF Jr., Heparan Sulfate Regrowth Profiles Under Laminar Shear Flow Following Enzymatic Degradation. Cell Mol Bioeng, 2013 6(2): p. 160–174. [PubMed: 23805169]

72. Ku DN, Giddens DP, Zarins CK, and Glagov S, Pulsatile flow and atherosclerosis in the human carotid bifurcation. Positive correlation between plaque location and low oscillating shear stress. Arteriosclerosis, 1985 5(3): p. 293–302. [PubMed: 3994585]

73. van den Berg BM, Spaan JA, Rolf TM, and Vink H, Atherogenic region and diet diminish glycocalyx dimension and increase intima-to-media ratios at murine carotid artery bifurcation. Am J Physiol Heart Circ Physiol, 2006 290(2): p. H915–20. [PubMed: 16155109]

74. Gouverneur M, Berg B, Nieuwdorp M, Stroes E, and Vink H, Vasculoprotective properties of the endothelial glycocalyx: effects of fluid shear stress. J Intern Med, 2006 259(4): p. 393–400. [PubMed: 16594907]

75. McDonald KK, Cooper S, Danielzak L, and Leask RL, Glycocalyx Degradation Induces a Proinflammatory Phenotype and Increased Leukocyte Adhesion in Cultured Endothelial Cells under Flow. PLoS One, 2016 11(12): p. e0167576. [PubMed: 27907146]

76. Lipowsky HH, Lescanic A, and Sah R, Role of matrix metalloproteases in the kinetics of leukocyte-endothelial adhesion in post-capillary venules. Biorheology, 2015 52(5–6): p. 433–45. [PubMed: 26600267]

77. Huang RB and Eniola-Adefeso O, Shear stress modulation of IL-1beta-induced E-selectin expression in human endothelial cells. PLoS One, 2012 7(2): p. e31874. [PubMed: 22384091]

78. Schengrund CL, Lausch RN, and Rosenberg A, Sialidase activity in transformed cells. J Biol Chem, 1973 248(12): p. 4424–8. [PubMed: 4351222]

79. Bosmann HB and Hall TC, Enzyme activity in invasive tumors of human breast and colon. Proc Natl Acad Sci U S A, 1974 71(5): p. 1833–7. [PubMed: 4365573]

80. Vlodavsky I, Elkin M, Abboud-Jarrous G, Levi-Adam F, Fuks L, Shafat I, and Ilan N, Heparanase: one molecule with multiple functions in cancer progression. Connect Tissue Res, 2008 49(3): p. 207–10. [PubMed: 18661344]

81. Chen Q, Jin M, Yang F, Zhu J, Xiao Q, and Zhang L, Matrix metalloproteinases: inflammatory regulators of cell behaviors in vascular formation and remodeling. Mediators Inflamm, 2013. 2013: p. 928315. [PubMed: 23840100]

82. Kurzelewski M, Czarnowska E, and Beresewicz A, Superoxide- and nitric oxide-derived species mediate endothelial dysfunction, endothelial glycocalyx disruption, and enhanced neutrophil adhesion in the post-ischemic guinea-pig heart. J Physiol Pharmacol, 2005 56(2): p. 163–78. [PubMed: 15985700]

83. Markovic S, Li B, Pera V, Sznaier M, Camps O, and Niedre M, A computer vision approach to rare cell in vivo fluorescence flow cytometry. Cytometry A, 2013 83(12): p. 1113–23. [PubMed: 24273157]

84. Markovic S, Li S, and Niedre M, Performance of computer vision in vivo flow cytometry with low fluorescence contrast. J Biomed Opt, 2015 20(3): p. 035005. [PubMed: 25822954]

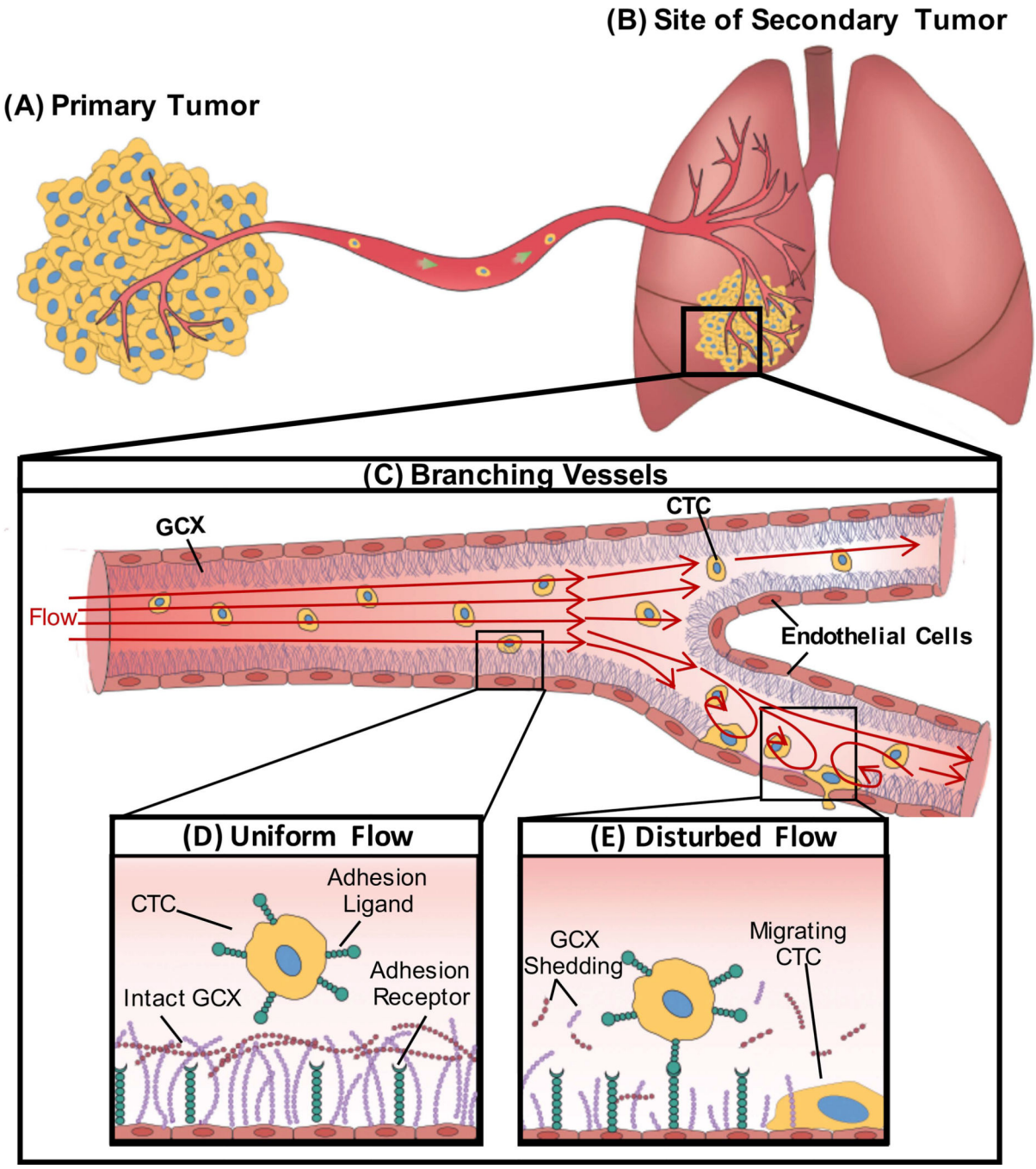

Figure 1:

A schematic showing the effect of DF patterns on endothelial GCX and circulating cancer cell attachment to the endothelium. **A**. Cancer cells within the primary tumor gain migratory properties and leave the primary tumor, intravasate through a nearby blood vessel, enter the bulk flow, and **B.** form secondary tumor sites in distant organs including the lungs. **C.** Geometric changes within the blood vessel results in different flow patterns. **D.** UF regions of blood vessels are known to have intact GCX resulting in the inability of CTC to attach to

the endothelium. **E**. Branched areas will produce DF; we hypothesize that this DF will result in degradation of the endothelial GCX enhancing attachment of CTC to the endothelium.

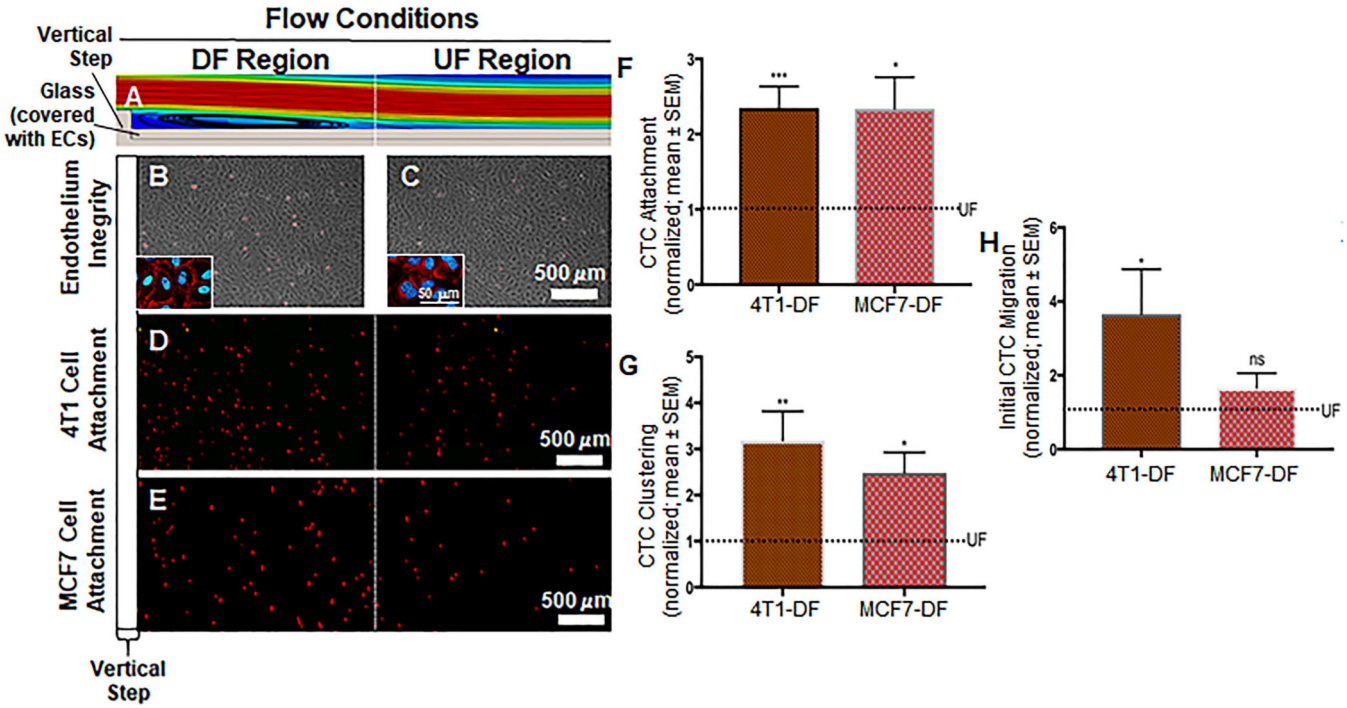

Figure 2:

A. A glass slide covered with ECs was placed at the bottom of the flow chamber. The ECs were exposed to a dynamic flow pattern that was generated by the introduction of a vertical step in the flow path. This computer aided simulation shows some of the flow pattern features. Here, the DF region is exaggerated for illustration purposes. It can be seen that eddy currents form immediately after the step, which is characterized by flow detachment, eddy current and reattachment sections. In addition, the DF region includes a transition in which the flow gradually adapts until it becomes UF. The transition region is followed by the UF region where the flow is void of any disturbances. Additional details can be found in Fig. S2 and its caption. **B and C**. Phase contrast images indicating healthy HUVEC monolayer after the introduction of both DF and UF. Insets show VE-cadherin labeled cells as further indication that endothelial layer is still intact in both DF and UF. **D and E**. Attachment of 4T1 breast cancer cells (D; red dots) and MCF7 cells (E; red dots) to the endothelium respectively. As expected cancer cells preferred to attach to the DF area than the UF area. **F.** Number of 4T1 and MCF7 breast cancer cells attached to the DF-conditioned endothelium. The dotted line represents normalized UF data. Significant increase in the attachment of cancer cells in the DF region compared to UF region. **G**. Number of cancer cell clusters formed in the DF region. The dotted line represents normalized UF data. We observed a significant increase in the clustering of 4T1 and MCF7 breast cancer cells to the endothelium in comparison with UF regions. **H**. Initial migration of 4T1 and MCF7 breast cancer cells through the DF-conditioned endothelium. The dotted line represents normalized UF data. Compared to UF regions, we observed a significant increase in the initial migration of cancer cells through the DF region, compared to UF areas. All data “Normalized with UF”. Student *t* test was used to compare DF vs. UF. Sample sizes: 4T1 attachment N=9,

MCF7 attachment N=5. Significance is compared to the UF condition and denoted as *P<0.05, **P<0.01, ***P>0.001, or not significant (ns).

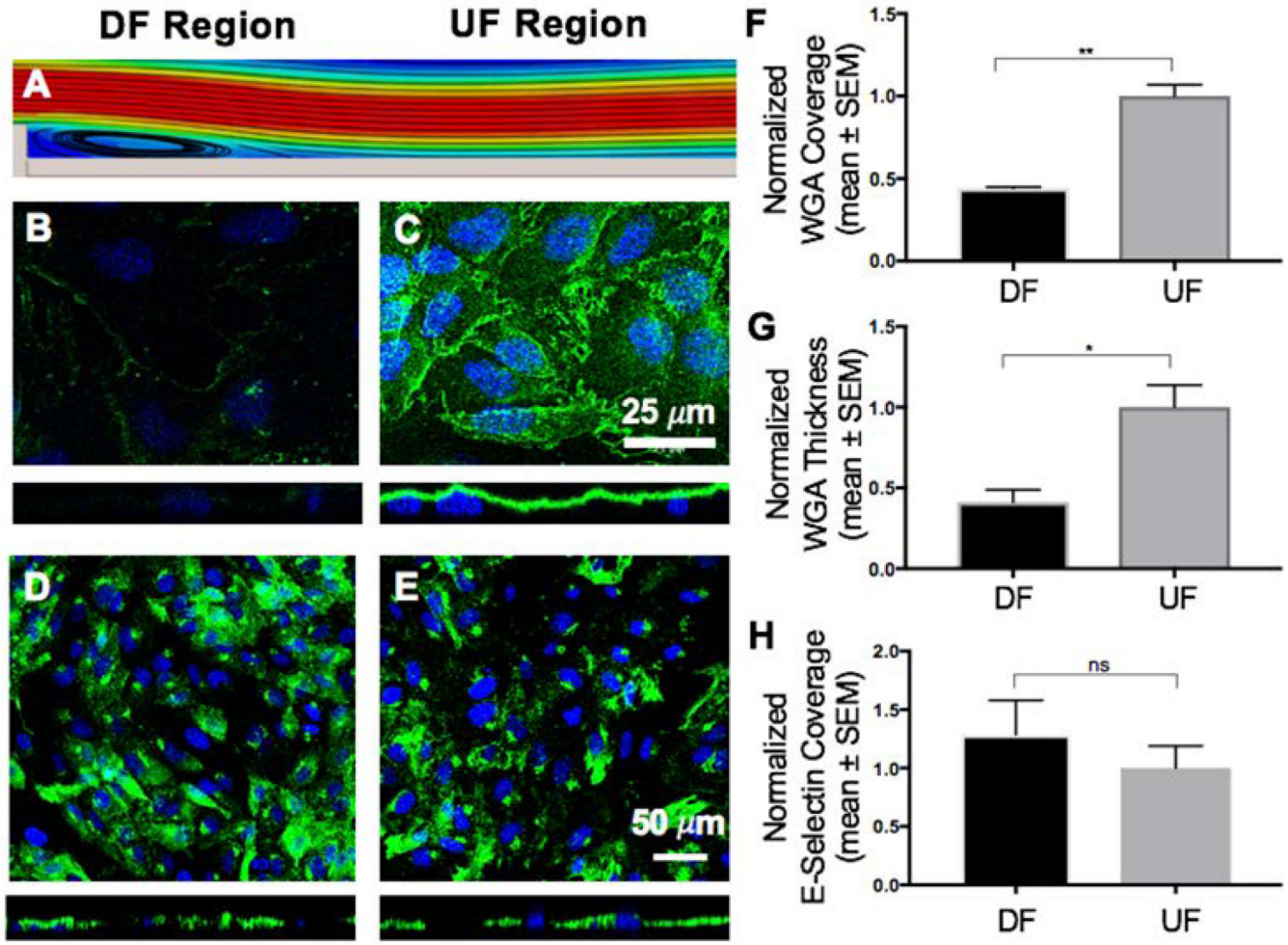

Figure 3:

Effect of DF and UF patterns on the GCX and the expression of E-selectin. **A**. Computer aided simulation of DF formation immediately after the step (refer to Fig. 2A and Fig. S2 for more details). **B**. The coverage and thickness of GCX is significantly low within the DF region (green is WGA-labeled GCX and blue is DAPI-labeled nuclei). **C**. In the UF region the GCX is shown to be abundantly expressed both in coverage and thickness. **D and E**. Expression of the endothelial surface adhesion molecule E-selectin. The introduction of different flow patterns did not affect the coverage of HUVEC by E-selectin. **F, G and H.** Data quantification for GCX coverage, GCX thickness, and E-selectin coverage, respectively, on the surface of HUVEC. **F**. GCX coverage in UF region compared to DF region. **G**. GCX thickness in UF region compared to DF region. **H**. E-selectin coverage in UF region compared to DF region. All data “Normalized with UF”. Student *t* test was used to compare DF vs. UF. Sample sizes: WGA-labeled GCX expression N=3, E-selectin expression N=9. Significance is denoted as *P<0.05, **P<0.01, or not significant (ns).

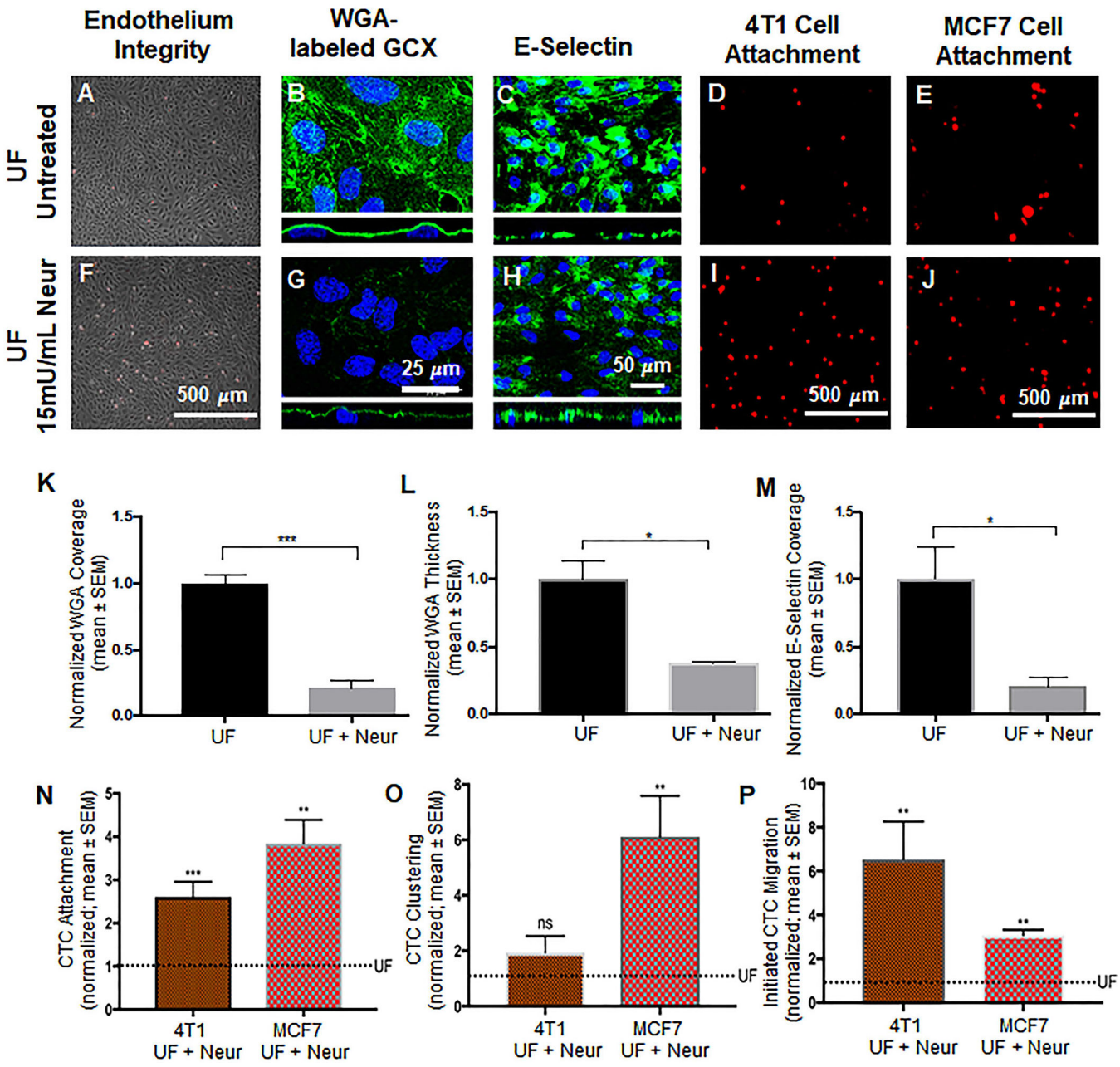

Figure 4:

Effect of the presence of Neur on cancer attachment, GCX expression, and E-selectin coverage. **A and F**. Phase contrast images revealing intact and healthy HUVEC monolayers in untreated conditions and after treatment with Neur. **B and G.** WGA-labeled GCX in UF (B) regions is abundant. Addition of Neur enzyme to the UF environment (G) abolishes WGA-labeled GCX. **C and H.** Coverage of HUVEC by E-selectin in conditions of isolated UF versus conditions of UF together with Neur enzyme. **D and I**. Attachment of 4T1 cells to HUVEC in UF region, prior to or after the introduction of 15mU/mL of Neur. **E and J**. Attachment of MCF7 cells to HUVEC in UF region, prior to or after the introduction of 15mU/mL of Neur. **K and L**. The quantification of coverage and thickness of GCX labeled

by WGA, respectively. **M**. Coverage of E-selectin in UF with enzyme treatment, compared to UF conditions. **N, O, and P.** Data quantification of the attachment, clustering and the initial migration of 4T1 and MCF7 breast cancer cells to HUVEC monolayers, respectively. All data are normalized with UF results. Student's *t* test was used to compare "UF" vs. "UF + Neur". Sample sizes are as follows: GCX expression N=3, E-selectin coverage N=6, 4T1 data N=7, MCF7 data N=4. Significance is denoted as *P<0.05, **P<0.01, ***P<0.001, or not significant (ns).

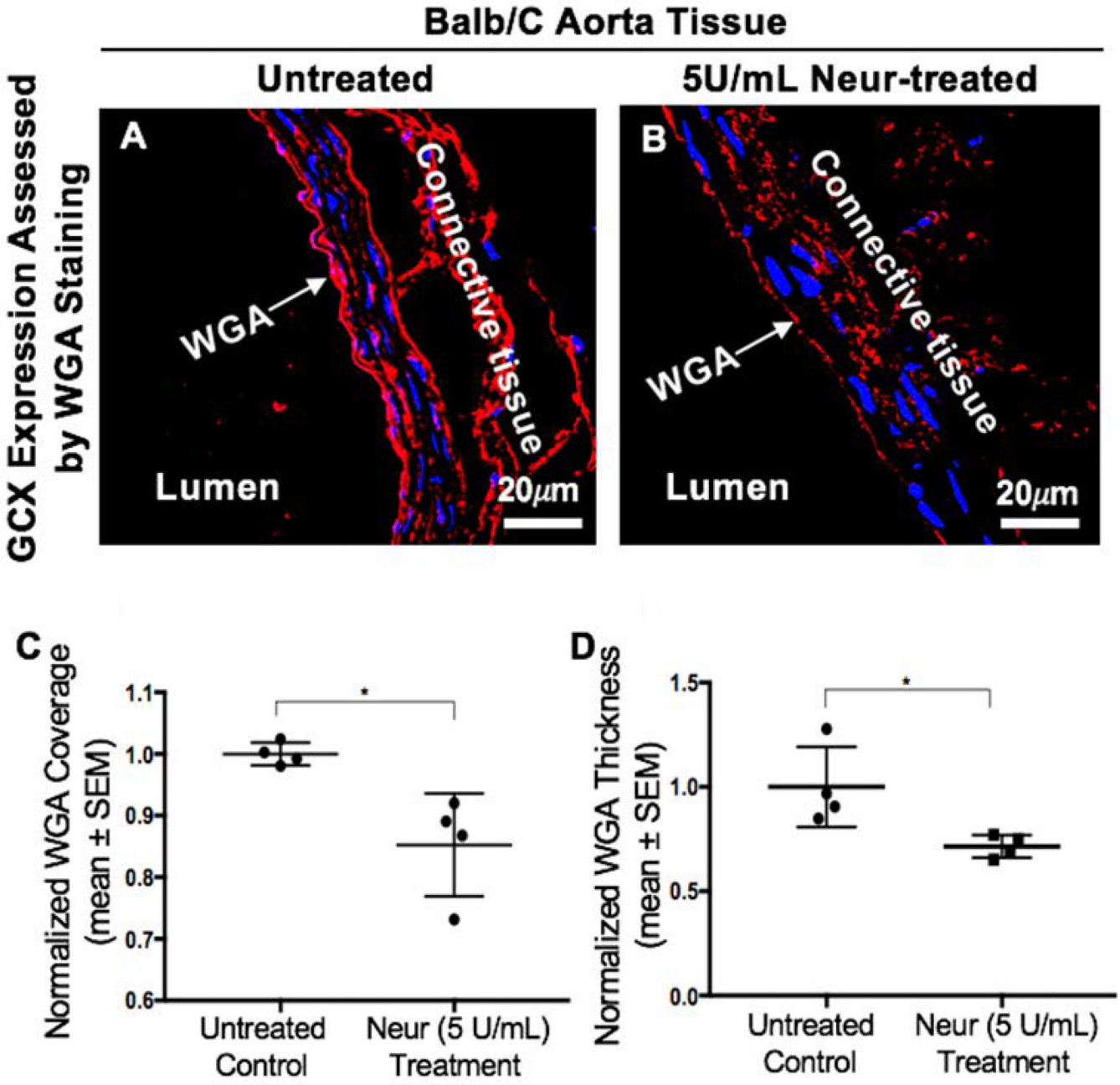

Figure 5:

Expression of GCX in the abdominal aorta of Balb/c mice. **A**. Control mice showing a uniform layer of GCX within the lumen of the abdominal aorta. **B**. After treatment of Balb/c mice with 5 U/mL of Neur we observed a decrease in the expression of GCX, with the layer showing discontinuity in coverage across the lumen of the abdominal aorta. **C**. Data quantification for coverage of GCX. **D.** Data quantification for the thickness of GCX. The sample size (N) is 4 for WGA-labeled GCX, data was statistically analyzed using the student t-test, and the statistical significance between the two groups is denoted as *P<0.05.

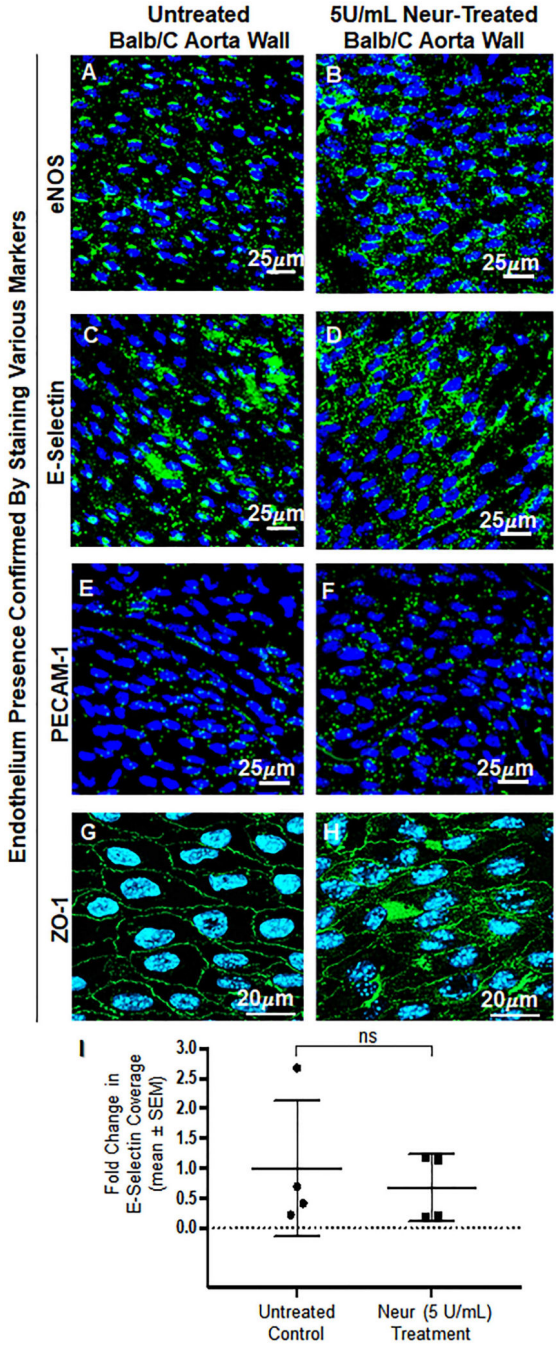

Figure 6:

En face confirmation of intact endothelium after treatment with 5 U/mL of Neur. **A and B**. Expression of eNOS before and after the treatment with Neur enzyme. Images show that eNOS is expressed around the nucleus of ECs. **C and D**. E-selectin coverage before and after the treatment with enzyme. E-selectin is expression across the surface of the endothelium. **E and F**. PECAM-1 staining before and after the treatment of enzyme. Visual inspection show the presence of PECAM-1 across the entire surface of the endothelium. **G and H**. ZO-1 staining before and after enzyme treatment. Images show the endothelial cell-

cell boundaries clearly and confirm endothelial barrier integrity. **I.** Data quantification for E-selectin showing a non-significant difference in expression of E-selectin on the endothelium between control and enzyme treated mice. All data are normalized with UF results. Student's *t* test was used to compare endothelium from untreated mice to endothelium from Neur-treated mice. The sample size (N) is 4. NS denotes "not significant".

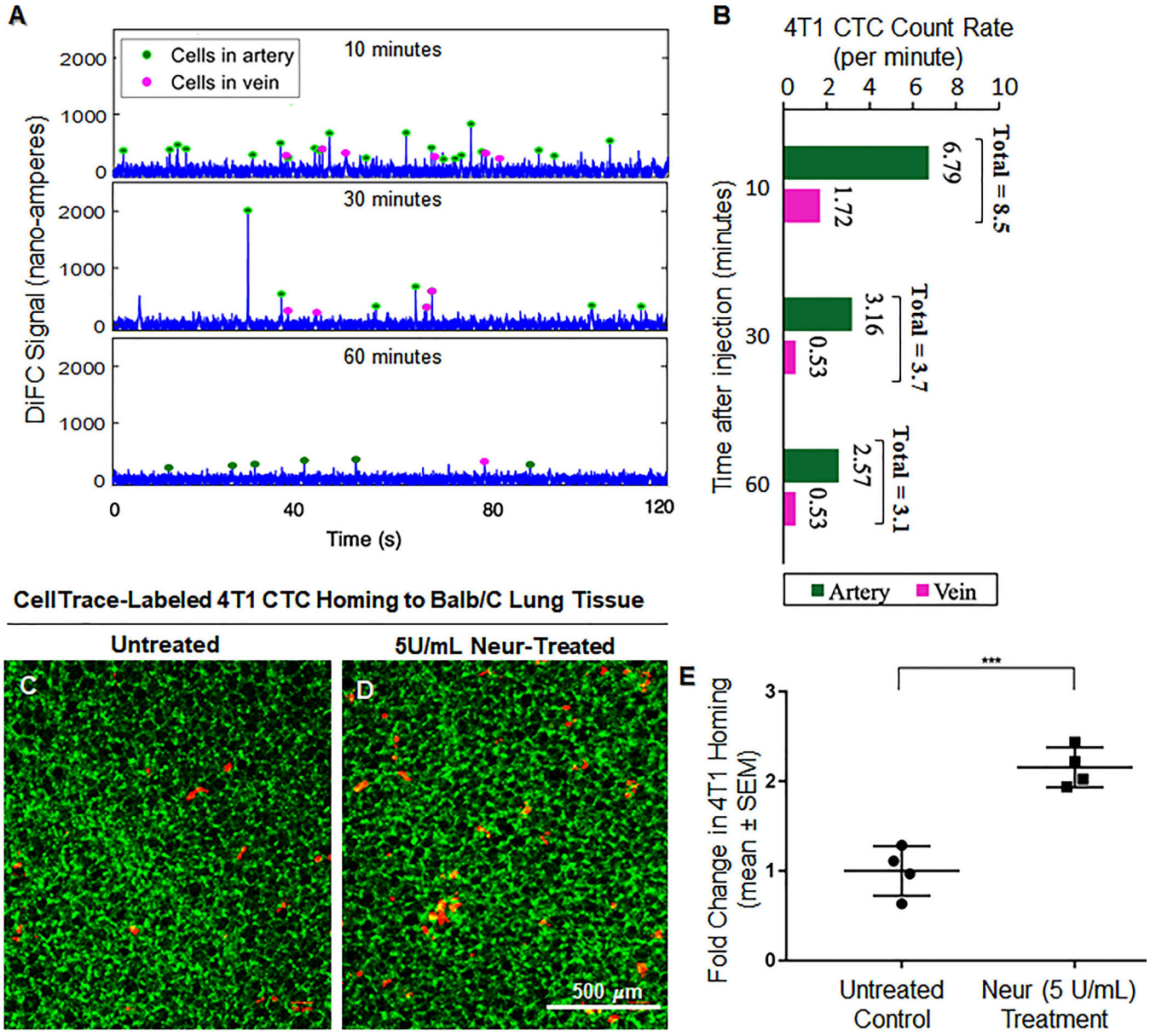

Figure 7:

In vivo attachment of 4T1 breast cancer cells to the lungs of BALB/C mice. **A and B.** *In vivo* data detected on diffuse *in vivo* flow cytometry (DiFC) system. Representative 120-second sequences of DiFC data show the number of cells in blood flow is decreasing over time after injection (A). The average CTC count rates detected in ventral caudal artery and ventral caudal vein and calculated in 15-minutes intervals, according to previously published methods [45], is also shown (B). **C**. Untreated control mice showing a limited attachment of 4T1 cancer cells to the lungs (green is the lung tissue and red dots are 4T1 breast cancer cells). **D**. We observed an increase in the attachment of 4T1 breast cancer cells to the lungs of BALB/C mice treated with 5U/mL of Neur. **E**. Data quantification showing a statistically significant increase in the attachment of 4T1 breast cancer cells to the lungs of BALB/C mice after treatment with 5U/mL of Neur. The sample size (N) is 4, data was statistically

analyzed using the student t-test, and the statistical significance between the two groups is denoted as ***P<0.001.